Title:

Allosteric mechanism of signal transduction in the two-component system histidine kinase PhoQ

Bruk Mensa[1,2], Nicholas F. Polizzi[1], Kathleen Molnar[1], Andrew Natale[1,3], Thomas Lemmin[4], William F. DeGrado[1]

[1] Department of Pharmaceutical Chemistry, University of California, San Francisco, CA 94158
[2] Chemistry and Chemical Biology program, University of California, San Francisco, CA 94158
[3] Cardiovascular Research Institute, University of California, San Francisco, CA 94158, USA
[4] Euler Institute, Università della Svizzera italiana, Ch-6900 Lugano, Switzerland

Abstract

Transmembrane signaling proteins couple extracytosolic sensors to cytosolic effectors. Here, we examine how binding of Mg^{2+} to the sensor domain of an *E. coli* two component histidine kinase (HK), PhoQ, modulates its cytoplasmic kinase domain. We use cysteine-crosslinking and reporter-gene assays to simultaneously and independently probe the signaling state of PhoQ's sensor and autokinase domains in a set of over 30 mutants. Strikingly, conservative single-site mutants distant from the sensor or catalytic site strongly influence PhoQ's ligand-sensitivity as well as the magnitude and direction of the signal, endowing diverse signaling characteristics without need for epistasis. Data from 35 mutants are explained by a semi-empirical 3-domain model in which the sensor, intervening HAMP, and catalytic domains can adopt kinase-promoting or inhibiting conformations, that are in allosteric communication. The catalytic and sensor domains intrinsically favor a constitutively 'kinase-on' conformation, while the HAMP favors the 'off' state; when coupled, they create a bistable system responsive to physiological [Mg^{2+}]. Mutants alter signaling by locally modulating these intrinsic equilibrium constants and couplings. Our model suggests signals transmit via interdomain allostery rather than propagation of a single concerted conformational change, explaining the diversity of signaling structural transitions observed in individual HK domains.

Introduction

Two component system sensor Histidine Kinases (HKs) are a conserved signaling module in bacteria responsible for sensing a myriad of environmental stimuli and orchestrating transcriptional responses along with their cognate transcription factors (Response Regulator, RR) (1,2). These sensors are generally implicated in environment sensing, and are involved in multi-drug resistance (3–5) and as master regulators of virulence programing in pathogenic bacteria (6,7). HKs are constitutive homodimers, which transmit signals through a series of intermediary domains to a cytoplasmic catalytic domain. While the lack of a full-length HK structure has hampered our understanding of the mechanism of signal transduction in these proteins, cytoplasmic domain structures have shed light particularly on the enzymatic core of this class of kinases. Several crystallographic snapshots of the autokinase domains of multiple HKs in various conformations (8–14), particularly CpxA, DesK, and VicK, have shown distinct conformations involved in autophosphorylation, phosphotransfer and dephosphorylation that may be conserved across this family. While these structures offer a conserved view of the catalytic cycle of the cytosolic autokinase domain (15), the question of how these proteins couple a sensory event on the other side of the membrane, and many nanometers away to the modulation of the activity of this domain remains unanswered.

This question is especially perplexing in light of the various modular architectures of HKs, involving the insertion of one or more signal transduction domains between sensors and the conserved autokinase domain. It is abundantly clear that the same conserved autokinase domain that defines this protein class can be regulated by a myriad of structural inputs, ranging from short alpha-helical dimeric coiled coils, to well-folded tertiary folds such as HAMP, PAS and GAF domains (16,17) (**Figure 1**). Moreover, it is clear from the representation of these folds in

diverse protein classes that these domains evolved independently of HKs and were co-opted pervasively into functioning HK architectures. Therefore, they are likely to serve a generalizable function that is robust to evolutionary selection, and the construction of physiologically relevant sensors optimally positioned to respond to environmental changes. While some intervening transduction domains have clearly annotated functions, such as the binding of intracellular ligands which are integrated into the sensory function of the HK, the requirement for other signal transduction domains remains obscure.

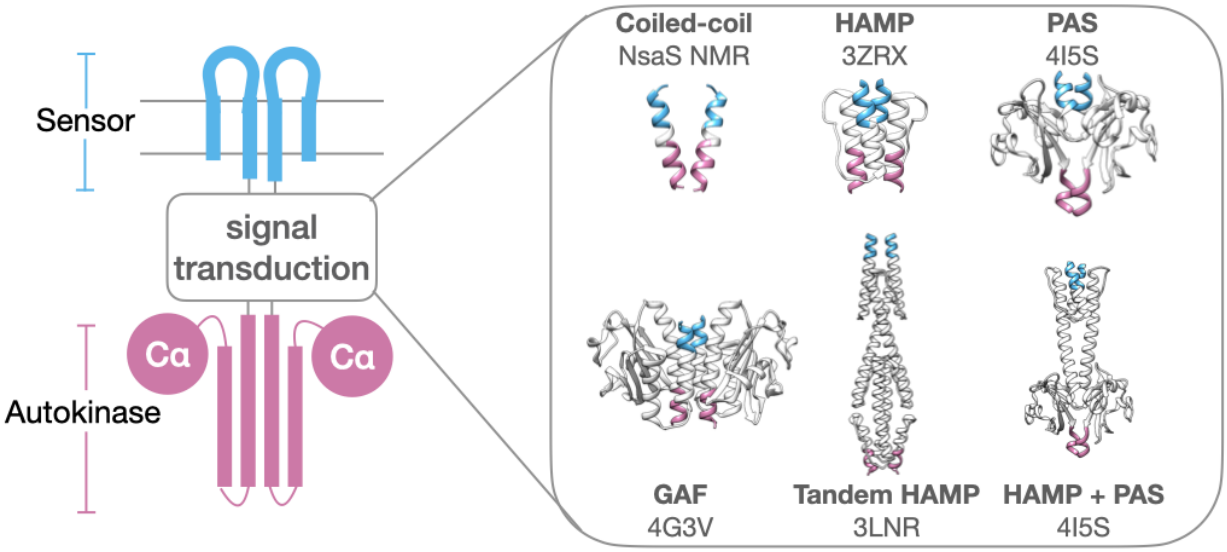

Figure 1 - Modular architecture of histidine kinases. Various protein folds and numbers of signal transduction domains are found inserted between sensor (blue) and autokinase (purple). Structurally elucidated examples include simple coiled-coils (NsaS), HAMP (AF1503), PAS (VicK), GAF (Nlh2), Tandem HAMP (Aer2) and HAMP/PAS domain (VicK). Pdb codes are provided in figure, except for NsaS (NMR structure).

In this work, we evaluate the coupling of sensor and autokinase domains in a model Gram-negative HK, PhoQ (18), in which these domains are separated by intervening transmembrane and HAMP signal transduction domains. The PhoQP two-component system is composed of a canonical transmembrane sensor HK, PhoQ, that senses the presence of divalent cations (19,20) and polycationic species such as antimicrobial peptides (21,22), and a cognate response regulator, PhoP (18,23), which transcriptionally controls regulons pertinent to cation transport and outer-membrane remodeling (24–33). The kinase activity of PhoQ is repressed by

73 divalent cation binding, whereas it is enhanced by the presence of antimicrobial peptides. PhoQ
74 is additionally implicated in low pH sensing (34) via an interaction with the membrane protein
75 UgtL (35), and has more recently been suggested to respond to changes in osmolarity (36),
76 although the mechanism is unclear. With respect to its most well characterized function, i.e., the
77 sensing of divalent cations such as Mg^{2+}, it is hypothesized that in the absence of such cations,
78 the electrostatic repulsion between an acidic patch in the sensor domain and the negatively
79 charged bacterial inner membrane enforces the 'kinase-on' conformation of the sensor and
80 results in high-kinase/ low-phosphatase activity in the autokinase domain. In the presence of
81 divalent cations, the electrostatic interaction between the sensor and inner-membrane are
82 bridged, resulting in a different 'kinase-off' sensor conformation that corresponds to low-kinase/
83 high-phosphatase autokinase function (37,38).
84 To probe the coupling between the sensor and autokinase domains, we established two
85 assays, which allow simultaneous measurement of the conformational states of the sensor and
86 autokinase domains (**Figure 2A**). Like most HKs, PhoQ is a constitutive parallel homodimer, in
87 which the individual domains interact along a series of coaxial helical bundles. Previously, we
88 observed that a Tyr60 → Cys variant forms interchain disulfides between the two monomers
89 only in the absence of Mg^{2+} where the protein is in the 'kinase-on' state. Thus, the fraction of the
90 sensor in the 'kinase-on' versus 'kinase-off' state can be readily quantified based on the amount
91 of dimer versus monomer seen in a western blot. Importantly, the Y60C substitution is minimally
92 perturbing, as the [Mg^{2+}] dependent signaling curve for this mutant is nearly identical to wild
93 type PhoQ with respect to the midpoint of the transition and activity of the basal and activated
94 states. Also, the redox environment of the periplasm of *E. coli* is buffered such that disulfide
95 formation is reversible and hence a good readout of the conformational state of the sensor. To

quantify the activity of the auto-kinase domain, we use a well-established beta-galactosidase gene-reporter assay that employs the PhoQ/PhoP-controlled promoter of the Mg^{2+} transporter MgtA. Although this assay is indirect, there is a reasonable correlation between promoter activity and PhoP phosphorylation (39). We note that similar assays have been extensively used by Falke, Haselbauer et al. (40) to probe signal transduction in chemosensors that are related to PhoQ.

Using this approach, we evaluate the extent to which the sensor's conformational state couples to and dictates the conformational activity of the autokinase domain for a set of over 30 mutants, representing substitutions throughout the signal transduction pathway from the sensor to the autokinase domain. We show how these mutants can modulate the three basic characteristics of a PhoQ signaling response which need to fit the biological role of the HK- the signal strength at the limiting high and low [Mg^{2+}], and the midpoint of the [Mg^{2+}] dependent transition- over the physiologically relevant concentration ranges that *E. coli* encounters (0.1- 10 mM). We further evaluate the intrinsic signaling equilibria of the sensor and autokinase domains by disrupting the allosteric coupling between them using poly-glycine insertions in the signal transduction pathway and show that both domains are highly biased to the 'kinase-on' state when uncoupled from each other. The intervening HAMP domain serves as a negative allosteric modulator of both these domains balances the stability of the 'kinase-on' and 'kinase-off' states, so that they can become responsive to physiological concentrations of Mg^{2+}. With these concepts in mind, we establish, fit and evaluate a semi-empirical 3-domain allosteric coupling model to account for the sensor-autokinase coupling and high/low asymptote and midpoint of transition behaviors of 35 distinct point-mutant and poly-glycine insertions, and highlight the advantages of inserted signal transduction domains in robustly modulating the signaling behavior of HKs.

Results

In the following sections, we first show how amino acid substitutions alter the signaling of PhoQ to induce a variety of outputs (**Figure 2**). We focus primarily on Ala substitutions at regions expected to be on the interior of the protein, and hence likely to alter the relative energetics of the kinase-promoting versus states. We also examined the effects of Trp substitutions in the TM helix at positions expected to map to the headgroup region of the biolayer, as similar substitutions often induce changes in signaling **(41)**. We avoid substituting residues in the entire autokinase domain or residues in the sensor that are involved in Mg^{2+} binding.

For each of the 35 variants, Mg^{2+}-dependent dose-response curves were evaluated for both transcriptional activation and crosslinking and were found to exhibit a rich range of behavior. Representative curves are shown in **Figure 2C**, and the entire collection of curves are shown in sections below. We seek the simplest allosteric model that can explain the entire gamut of phenotypes, by evaluating a series of simple allosteric models of increasing complexity. In the next sections, we use theoretical curves to qualitatively show the limitations of the simplest models. Ultimately, we develop a 3-domain model with variable coupling between the domains, which is sufficient to fully explain the entire range of activities of all 35 mutants.

Fully cooperative two-state models are unable to explain the gamut of activities of mutants

The simplest model for signaling in HKs is one in which the entire HK exists in a two-state equilibrium of 'kinase-on' and 'kinase-off' states which is then modulated by ligand binding (**Figure 2B**). In the case of PhoQ, Mg^{2+} binding stabilizes the 'kinase-off' state. As such, the fraction of PhoQ that is 'kinase-on' at any given $[Mg^{2+}]$ is equal to the fraction of PhoQ that is ligand-free. In such a model, the upper asymptote of activity at low $[Mg^{2+}]$ ($[Mg^{2+}] << K_d$) is

142 governed by K, the two-state equilibrium for the kinase-on versus kinase-on conformations (
143 f(active) ≈ K/(1+K), see **Figure 2** for definition of symbols). In the models considered in this
144 paper, we assume that Mg^{2+} binds to single sites in the sensor domains. It is possible that binding
145 between the sites is cooperative or that more than one Mg^{2+} ions are bound per domain.
146 However, given the fact that the transcriptional assay is an indirect readout of the 'kinase-on'
147 state, and as such is not necessarily perfectly linear with respect to the fraction of activation, we
148 are not able to differentiate between models that differ subtly in their dose-response curves.
149 However, our data (see below) are able to rule out highly cooperative models in which many
150 binding sites must be occupied with high cooperativity (as in the Asp receptor (42)) as this would
151 result in a much sharper dose-response curve. In the simple two-state model, the lower
152 asymptote, PhoQ will always be pushed to a fully 'kinase-off' state at high enough $[Mg^{2+}]$
153 ($[Mg^{2+}] >> K_d$) because the fraction of autokinase in a given signal state is equivalent to the
154 fraction of sensor in the corresponding state. The midpoint of transition is dictated by the relative
155 magnitudes of K, which reflects the relative preference for the 'kinase-on' vs. 'kinase-off' state,
156 as well as K_d, which is the affinity of Mg^{2+} for the 'kinase-off' state, as shown in **Figure 2B**.
157 Since the model does not allow for any decoupling of sensor and autokinase domains, the
158 fraction of sensor that is crosslinked is identical to that of the autokinase in the 'kinase-on'
159 conformation.

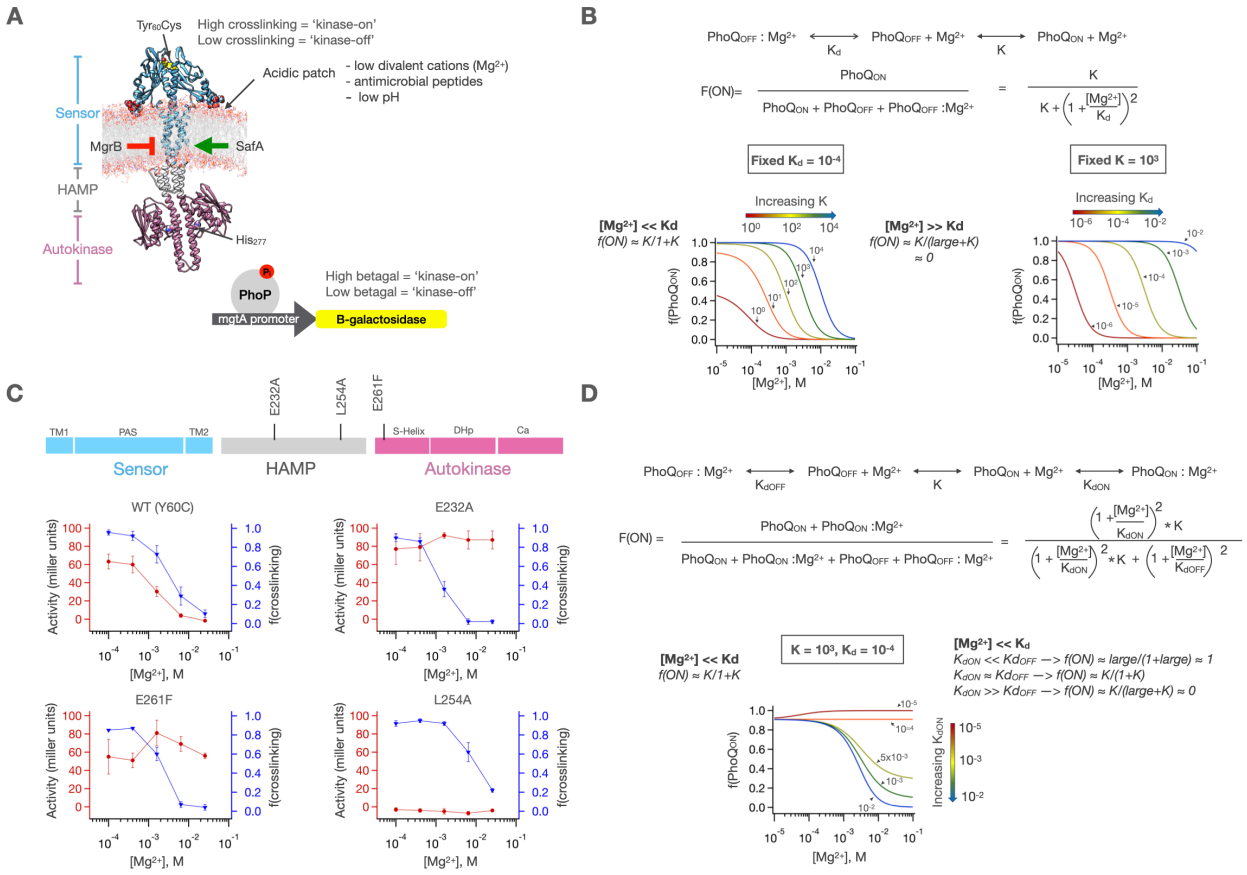

Figure 2 – A fully concerted signaling mechanism does not explain PhoQ activity. A) MD model of PhoQ in which the sensor (res. 1-219, blue), HAMP (res. 220-260, grey) and autokinase domains (res 261-494, purple) are annotated. The sensor contains a Y60C mutation (spheres) which shows signal state dependent crosslinking. The autokinase contains the conserved catalytic His277, which upon phosphorylation transfers inorganic phosphate to the response regulator PhoP, which then modulates a *mgtA* promoter-driven beta-galactosidase reporter. Stimuli and regulatory proteins that modulate PhoQ activity are shown. **B)** A fully concerted (single domain) signaling scheme in which the intrinsic signaling equilibrium of PhoQ, K, is modulated by Mg^{2+} binding at affinity = K_d. While this model allows for modulation of the low [Mg^{2+}] asymptote and midpoint of transition, it does not allow for modulation of the high [Mg^{2+}] asymptote. **C)** sensor crosslinking and autokinase activity determined for 'wild type' (Y60C) PhoQ (n=9), as well as 3 mutations (n=2) along the signal transduction pathway. The sensor state and autokinase activity are not identically correlating as would be predicted by a concerted signaling mechanism. Error bars correspond to ±SD error **D)** Allowing both states of PhoQ to bind Mg^{2+} allows for modulation of all 3 features, but still maintains obligatory correlation between sensor and autokinase.

We next examined a large set of sensor and autokinase activities of 'wild type' (Y60C) PhoQ at 5 different concentrations of Mg^{2+} to evaluate whether they collectively deviate from the behavior expected for the simple two-state model. Illustrative data in **Figure 2C** show it is possible to have low levels of kinase-activity at low [Mg^{2+}] even though the sensor remains in a high-crosslinking kinase-on state (e.g. L254A). Similarly, some mutations retain high kinase-activity in the autokinase despite the sensor transitioning to a predominantly low-kinase (low-

crosslinking) state (e.g. E232A, E261F). Finally, some mutants produce higher levels of kinase activity at low-Mg^{2+} than 'wild type' PhoQ, demonstrating that even at the low-[Mg^{2+}] conditions in which the sensor is fully in the crosslinked 'kinase-on' state, there remains a significant fraction of the WT autokinase that remains in the 'kinase-off' state (e.g. E232A is more active than WT PhoQ at low [Mg^{2+}]). Therefore, this fully concerted signaling model is insufficient to describe the full range of activities of PhoQ variants.

It is possible to account for the variable kinase activity at high [Mg^{2+}] by considering a model in which allows Mg^{2+} to bind to both the 'kinase-on' and 'kinase-off' states with different affinities, analogous to Mg^{2+} itself behaving as a low-affinity inverse agonist of PhoQ (**Figure 2D**). Indeed, for the sensor of PhoQ, there is no reason to preclude ligand binding in either sensor state, since the same negatively charged surfaces are present in both states and can conceivably still bind Mg^{2+}, albeit at a much lower affinity due to the lack of bridging interactions (43). In this scenario, the 'kinase-off' asymptote at high [Mg^{2+}] is determined by the relative values of K_{dON} and K_{dOFF}, as shown in **Figure 2D**. However, this model cannot explain the large differences in the shapes of the curves seen for crosslinking versus reporter gene expression for the same mutant, as in **Figure 2C**. Such behavior requires an additional parameter that describes the degree of coupling between the sensor and autokinase domains.

Allosteric coupling between sensor and autokinase domains

A ligand-dependent sensor can be allosterically coupled to an autokinase domain with a tunable coupling strength to allow for the desired degree of communication between the sensor and the autokinase. In such a scheme, the sensor would be a ligand-binding domain with all the properties previously described for a fully concerted HK. The autokinase, in the absence of linkage to the sensor, would have a constant activity level based on its own intrinsic 'kinase off'

to 'kinase on' equilibrium. The sensor is then connected to the autokinase in a manner that biases the intrinsic autokinase equilibrium differently depending on which signaling state the sensor is in. A ligand-dependent allosterically modulated HK results from such a coupling, so long as sensor 'kinase-on' and 'kinase-off' states of the sensor alter the autokinase equilibrium differently. To reduce the number of parameters needed to describe such a model, we can define the intrinsic equilibria of the sensor and autokinase when they are connected to a reference state (e.g., 'kinase-off') with equilibrium constants as shown in **Figure 3A**. K_{Sen} is the 'intrinsic' equilibrium of the sensor domain when connected to an autokinase in the 'kinase-off' state, and K_{AK} is the 'intrinsic' equilibrium of the autokinase domain when connected to the sensor in the 'kinase-off' state. When coupled to the 'kinase-on' state of either domain, K_{Sen} and K_{AK} are scaled by a new factor, α. **Figure 3B-C** illustrate the effect of α on the Mg^{2+} dose-response curves. When $\alpha = 1$, the two domains are fully uncoupled, and the binding of Mg^{2+} to the sensor is unable to affect the autokinase domain (**Figure 3B**). A value of $\alpha>1$ means that when either of the domains switches to the 'kinase-on' state, the other domain's propensity to switch 'kinase-on' state is also enhanced by that factor, creating a correlated ligand-mediated transition between sensor and autokinase (**Figure 3C**). If $0<\alpha<1$, then a transition to 'kinase-on' state is actually easier when the other domain is in the 'kinase-off' state, creating an anticorrelated ligand dependent behavior. When the absolute value of the log of α becomes very large (i.e., when α is either $>>1$ or approaching zero), the two domains are highly coupled (**Figure 3D**) and the system behaves as in the fully concerted 2-state models in **Figure 2**. Therefore, α is the coupling strength between the 'kinase-on' states relative to the coupling between the 'kinase-off' states built into K_{Sen} and K_{AK}.

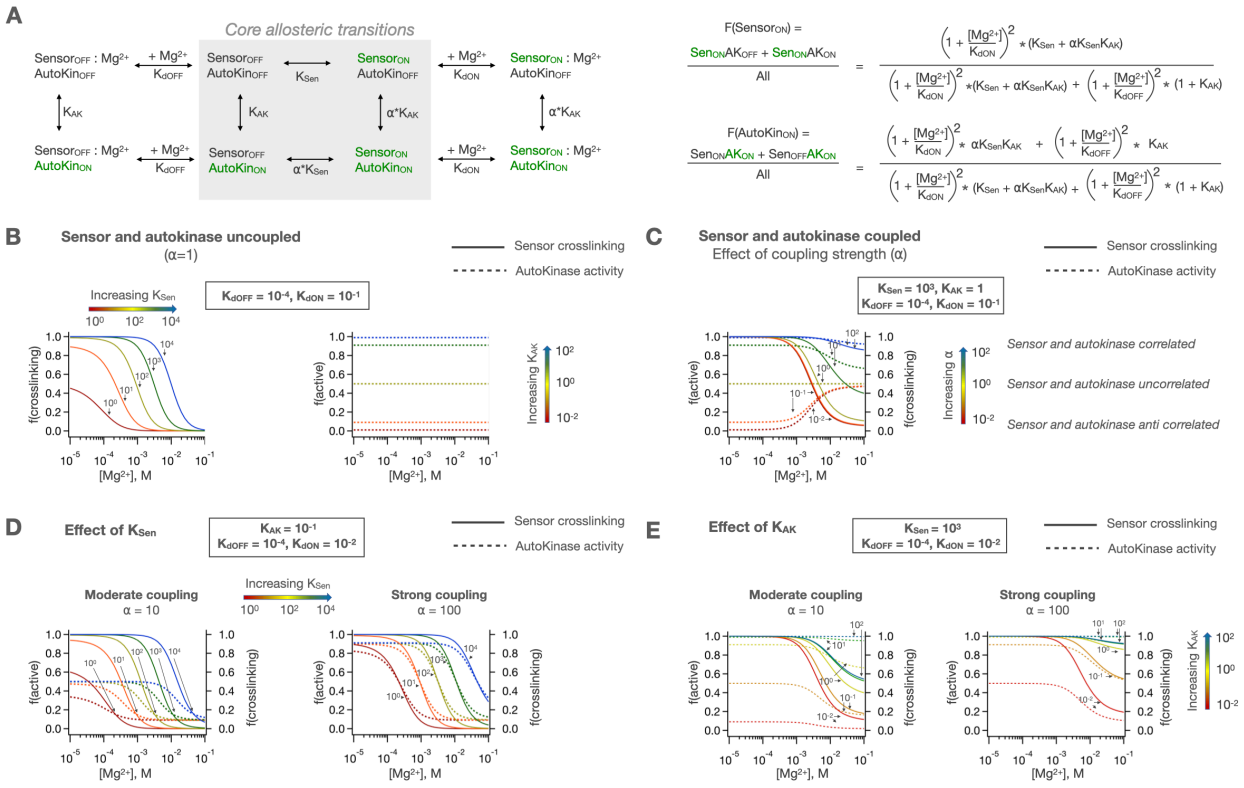

Figure 3 - A 2 domain coupling scheme for PhoQ signaling. A) The sensor and autokinase domains of PhoQ are allowed to sample both 'kinase-on' and 'kinase-off' states with equilibrium constants K_{Sen} and K_{AK} when the other domain is in the 'kinase-off' state. When the other domain is in the 'kinase-on' state, the equilibria are scaled by the coupling constant, α. This allows for semi-independent fractions of sensor and autokinase in the 'kinase-on' state, which are computed as shown. **B)** In the uncoupled case (α=1), K_{Sen} modulates the sensor identically to the previously described concerted signaling mechanism, while K_{AK} sets the basal autokinase activity. **C)** The coupling of these domains with α≠1 results in [Mg^{2+}] dependent activity that is either correlated (α>1) or anticorrelated (α<1). As α gets larger, the two domains act more as one concerted protein. **D)** Changes in the intrinsic equilibrium of the sensor affect autokinase activity through coupling, and similarly **E)** changes in the intrinsic equilibrium of the autokinase domain can alter the ligand-dependent crosslinking behavior of the sensor.

Coupling provides a robust mechanism for setting both the upper and lower activity asymptotes of the full-length sensor kinase. At high enough [Mg^{2+}], the low-crosslinking 'kinase-off' state of the sensor becomes dominant, and the corresponding activity of the autokinase will be dictated by the autokinase equilibrium when coupled to this 'kinase-off' state, K_{AK}. At low [Mg^{2+}], the high-crosslinking 'kinase-on' state of the sensor will be dominant, and the corresponding activity of the autokinase will be dictated by α*K_{AK}. The midpoint of transition will depend on the relative magnitudes of all the parameters. However, the range of behaviors possible by this model of coupling depends heavily on the intrinsic equilibria of the

246 sensor and autokinase themselves (K_{Sen}, K_{AK}). We next purposefully eliminated coupling
247 experimentally (α=1) to obtain estimates of K_{Sen} and K_{AK}, and to evaluate whether the 2-domain
248 allosteric coupling mechanism is feasible in PhoQ.

249 **The effect of decoupling the HAMP domain from the catalytic and sensor domains.**

250 The allosteric model in **Figure 3** predicts that when the sensor and autokinase domains
251 are fully uncoupled (α=1) these two domains act independently, i.e., the intrinsic equilibria of the
252 sensor (K_{Sen}) is the same irrespective of the state of the autokinase, and the equilibria of the
253 autokinase (K_{AK}) likewise becomes independent of the state of the sensor. To accomplish this
254 decoupling experimentally, we insert a stretch of 7 helix-disrupting glycines (Gly_7) to interrupt
255 the helical connections that are required for coupling between PhoQ's domains. One Gly_7
256 insertions was introduced just before the HAMP (Gly_7 -219/220) as the TM helix exits the
257 membrane. The other Gly_7 insertion (Gly_7 -259/260) was made just after the HAMP signal
258 transduction domain within a short helical connection to the autokinase domain. By comparing
259 the effects of these insertions, we can decipher the role of the intermediate HAMP domain in
260 signal propagation.

261 As expected, both mutants decouple Mg^{2+} binding from kinase activity (**Figure 4**).
262 However, they have markedly different effects on the sensor and catalytic domains when these
263 activities are evaluated individually. When the HAMP is decoupled from the sensor by
264 introducing the Gly_7 insertion between the HAMP and sensor domains, the sensor is highly
265 activated, and remains in the high-crosslinking state, even at concentrations of Mg^{2+} sufficient to
266 switch WT to the kinase-off state. On the other hand, if the HAMP remains coupled to the sensor
267 as in (Gly_7 -259/260) it behaves normally, being efficiently crosslinked in a [Mg^{2+}]-dependent
268 manner similar to WT. Thus, the HAMP would appear to favor the 'kinase-off' state, serving to

reset the energetics of the otherwise highly stable 'kinase-on' state of the sensor. The resulting coupling provides an energetic balance so the system can respond to Mg^{2+} over the physiological range. The HAMP has a similar influence on the catalytic domain. When the native connection between the HAMP and the catalytic domain is disrupted by Gly_7 insertion, it is highly activated. By contrast, when the connection between the HAMP and catalytic domains is retained as in WT, the kinase activity is strongly downregulated.

These findings show that the HAMP domain serves not solely as a passive element that transmits a signal between the sensor and autokinase, but also plays a more active role in modulating the energetics of otherwise constitutively-on sensor and kinase domains so that the overall protein becomes fully responsive to physiological $[Mg^{2+}]$. Thus, the HAMP domain serves as a separate, intervening domain with its own intrinsic equilibrium, in which the intrinsically preferred signaling state is negatively coupled to both sensor and autokinase.

We also see that the two-domain model in **Figure 3** captures much of the phenotypic behavior of the mutants. However, the fact that different effects are seen for decoupling before and after the HAMP indicates that it needs to be treated as a separate domain with its own equilibrium constant and coupling to both the sensor and catalytic domains. The treatment of the HAMP as a separate domain is of course parsimonious with its separate evolution as a bistable domain independent of histidine kinases, and its modular insertion into the various classes of proteins for which it is named. In subsequent sections we will additionally see this parsing into variably coupled domains can explain how mutations in the HAMP can modulate the sensitivity to Mg^{2+} and the dynamic range of PhoQ signaling.

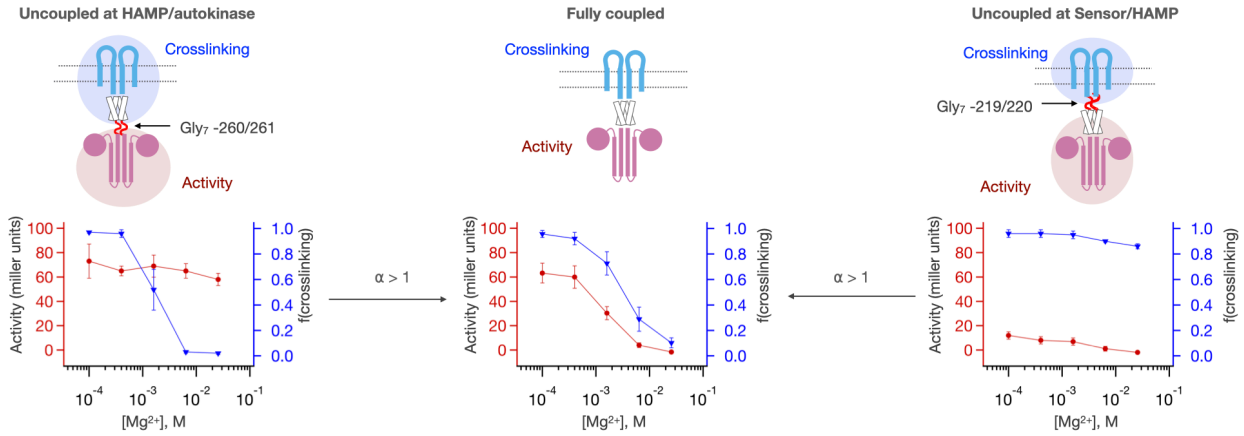

Figure 4 – Intrinsic activities of the PhoQ sensor and autokinase domains are altered by coupling to HAMP. Gly_7 disconnections are inserted either between the HAMP and the autokinase (Gly_7 - 260/261, left, n=3) or between the Sensor and HAMP (Gly_7 -219/220, right, n=2) to disrupt allosteric coupling between sensor and autokinase. Both the sensor and autokinase by themselves have high 'kinase-on' propensity. However, presence of the HAMP with either of these domains potentiates the 'kinase-off' state, resulting in a more [Mg^{2+}] responsive sensor, or a lower basal activity autokinase. These halves can be connected with positive allostery ($\alpha>1$) to result in the observed sensor/autokinase activity of fully coupled PhoQ (middle, n=9).

The HAMP domain is negatively coupled to the autokinase domains of CpxA and BaeS

Given the profound effect of the HAMP domain on the intrinsic activities of the PhoQ sensor and autokinase domains, we sought to examine if HAMP domains have similar effects in closely related but functionally distinct HKs with the same arrangement of signaling domains as in PhoQ. While we do not have facile means for evaluating the effect of the HAMP on sensor domains, we can examine the transcriptional activity of autokinase domains with and without coupling to their HAMP domains. We constructed Gly_7 insertions in two closely related *E. coli* HKs, CpxA and BaeS, that have very similar architectures to PhoQ (both have similarly arranged PAS sensor, antiparallel 4-helix TM, a single cytosolic HAMP, and the conserved autokinase domains). The HK CpxA responds to periplasmic protein misfolding stress via an accessory protein, CpxP, and upregulates genes to mitigate this stress, such as periplasmic proteases and chaperones and modulation of outer membrane porin expression (44–46). It is similar to PhoQ in that the free HK is kinase-active, and is turned off by the binding of the periplasmic CpxP protein (47). BaeS is a closely related HK, which has significant overlap with CpxA, both in the

inducing stimuli as well as the genes regulated (48). We evaluated the activity of these kinases using previously validated fluorescent gene-reporters (p*cpxP*::GFP for CpxA activity(49), p*spy*::mCherry for BaeS activity(50)) in a double CpxA/BaeS knockout strain. When the Gly_7 motif is inserted immediately upstream of the autokinase domain, we observe a high basal activity for both kinases similar to PhoQ (**Figure 5**). However, when the Gly_7 motif is migrated upstream of the HAMP thereby allowing the HAMP to couple to the autokinase, this high basal activity is potently repressed, again similar to PhoQ. This suggests that the HAMP strongly coupling to and altering the intrinsic activities of adjacent domains may be a generalizable principle, although it might not serve as a negative element in all cases.

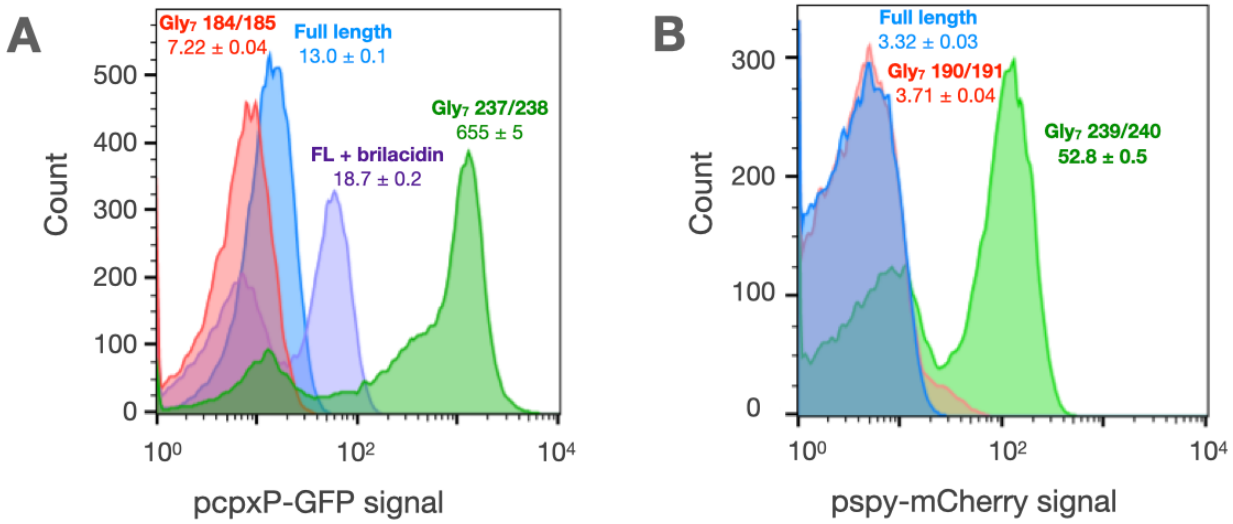

Figure 5 – Glycine disconnections in CpxA and BaeS. A) The activity of CpxA constructs is measured in AFS51 strain (Δ*cpxA*) using a p*cpxP*::GFP reporter. Wild type CpxA is responsive to the antimicrobial mimetic, brilacidin (purple histogram). The autokinase domain of CpxA in isolation shows very high kinase activity (green), which is repressed to basal levels by the addition of the HAMP domain alone (red). **B)** The activity of BaeS constructs is measured in a Δ*baeS* Δ*cpxA* strain using a p*spy*::mCherry reporter. The autokinase domain of BaeS shows high kinase activity (green), which is repressed by the addition of the HAMP domain alone (red). Median reporter fluorescence values ± STE (n=20,000) are reported below labels for single experiment.

Three-domain allosteric coupling mechanism of signal transduction

We next turned our attention to building a quantitative model that describes all the experimental data for 35 mutants. Based on the results of Gly_7 insertion mutants, we developed a three-domain model, with the boundaries defined before and after the HAMP. In this model, the

335 HAMP has its own intrinsic equilibrium, K_{HAMP}, and there are two coupling constants that
336 describe how the sensor couples to the HAMP (α_1), and how the autokinase couples to the
337 HAMP (α_2). All possible state transitions are enumerated in **Figure 6A**. This treatment allows
338 for semi-independent modulation of the sensor and autokinase using the intrinsic equilibrium of
339 the HAMP. In the case where $\alpha_2 = 1$, the autokinase is decoupled from the sensor + HAMP. In
340 this scenario, the HAMP can modulate the [Mg^{2+}] dependent state transition of the sensor
341 through coupling via α_1 without altering the basal autokinase activity, as shown in **Figure 6B**. In
342 the case where $\alpha_1 = 1$, the sensor is decoupled from the HAMP+autokinase, and the HAMP can
343 modulate the basal (and ligand-insensitive) activity of the autokinase through coupling via α_2, as
344 shown in **Figure 6B**. When the protein is fully coupled (i.e. $\alpha_1, \alpha_2 \neq 1$), we can potentiate the
345 'kinase-on' or 'kinase-off' states of the sensor and autokinase in a manner that depends on both
346 K_{HAMP} and α_n's, as shown in **Figure 6C**. Of particular interest is the case where $\alpha_1, \alpha_2 < 1$, which
347 enables the simultaneous potentiation of the 'kinase-off' state, while maintaining correlated
348 sensor-autokinase behavior as observed in our Gly_7 insertion experiments. Other possible
349 behaviors with this 3-domain model include correlated sensing with 'kinase-on' potentiation, and
350 anticorrelated signaling.

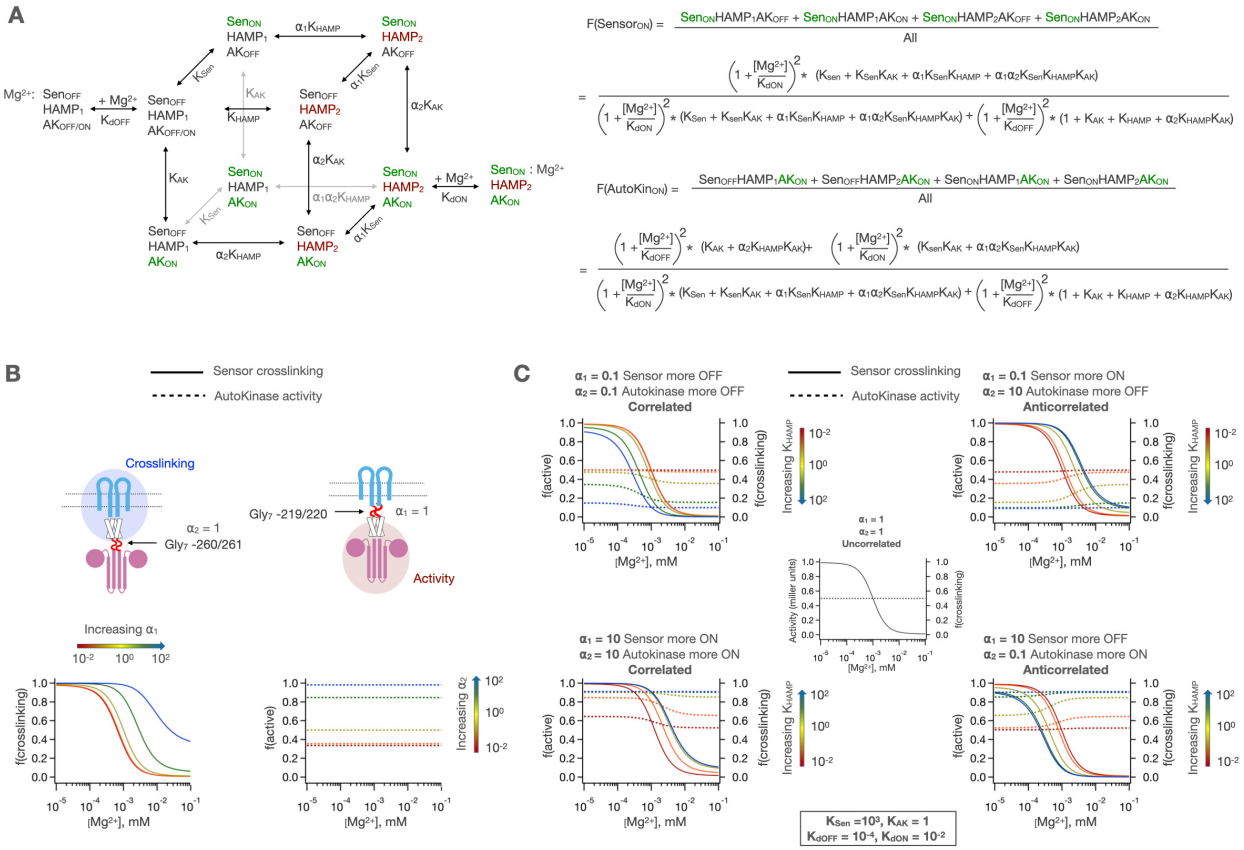

Figure 6 - 3-domain allosteric coupling model for PhoQ signaling. A) The sensor, HAMP and autokinase domains of PhoQ are allowed to sample both 'kinase-on' and 'kinase-off' signaling states while coupled to 'kinase-off' states in adjacent domains with equilibria K_{Sen}, K_{HAMP} and K_{AK} respectively. When adjacent states are in 'kinase-on' states, the equilibria for transition are scaled by α_1 (sensor-HAMP) or α_2 (HAMP-autokinase). Predicted fraction of sensor crosslinking or autokinase activity are computed as shown below. **B)** The HAMP allows for the independent modulation of the basal state of the sensor or autokinase. When $\alpha_2 = 1$, the HAMP modulates the $[Mg^{2+}]$ dependent transition of the sensor, and when $\alpha_1 = 1$, the HAMP modulates the basal activity level of the autokinase. **C)** the two allosteric coupling constants allow for both correlated and anticorrelated modulation of sensor and autokinase and allow for potentiation of both the 'kinase-on' and 'kinase-off' states.

In order to fit our semi-empirical models to experimental observations, we generated a set of 35 single-point mutants and Gly_7 insertions and *simultaneously* determined the sensor-crosslinking and autokinase activity at 5 different concentrations of Mg^{2+}. We sampled regions all along the signal-transduction pathway between the sensor and autokinase, including the dimeric interfacial helices of the sensor dimer, the 4-helix transmembrane domain, the HAMP, as well as the conserved S-Helix motif that couples the HAMP to the autokinase (**Figure 7A**).

Using this set of mutants, we next sought to determine the five core allosteric parameters (K_{Sen}, K_{HAMP}, K_{AK}, α_1, α_2), and the dissociation constants for Mg^{2+} to the two sensor states

(K_{dOFF}, K_{dON}). One last parameter (S) is a scaling factor that relates the mole fraction of autokinase in the 'kinase-on' state to the experimentally observed Miller units associated with the beta-galactosidase transcription (**Figure 6A**), which were obtained under strictly controlled experimental conditions to assure uniformity between mutants. In all, we sought to determine eight constants for each mutant. However, given the spacing of the points in our dose-response curves, it is only possible to obtain three pieces of information, i.e., the top, bottom and midpoint of the curves. Thus, with only six pieces of information (3 each from crosslinking and transcriptional activation) for each mutant, the model is under-determined for any one mutant. We avoid this problem by using global fitting. For a given mutant, only one or two (or in 1 occasion, three) of the parameters are allowed to vary, with the others being fit as global parameters that are shared with other mutants. The choice of which parameters to vary is determined by the location of the perturbation on the primary sequence of PhoQ (**Figure 7A**, see methods). For example, a mutant near the N-terminus of the HAMP domain would be expected to primarily alter α_1 and K_{HAMP}, so these values were allowed to vary locally. Mutants near the center of the tertiary structure of the HAMP domain are allowed to vary K_{HAMP} alone and so on. This results in an overall fit with 62 adjustable parameters corresponding to 8 global parameters, 47 locally varied parameters, and 7 parameters fixed to a value of 1 to account for Gly_7 insertions (**Table 1**). By comparison, there are 6 * 36 = 216 observables. Thus, in theory, the data should be more than sufficient to define the independent parameters.

This model was globally fit using our mutation dataset as explained in detail in the methods section. Briefly, we standardize the ranges of autokinase activity measurements (Miller units from beta-galactosidase assay) by the global average activity in our dataset. This normalizes the range of autokinase activity to one that is similar to crosslinking fractions (range 0 to 1) and

gives both types of experimental measurements similar weights in our global fits. We give additional weight to data with experimental replicates (and hence greater certainty) by simply treating each replicate as an independent data set, with all the variables held constant between replicates during fit. Each parameter is allowed to sample a 10-log range of possible values, and the best fit is determined by minimizing the sum of residuals across the entire dataset. In order to avoid getting trapped in any local minima of the parameter space, we repeat the fit 125,000 times using randomly generated starting values for each parameter and determine confidence intervals for our parameters using a bootstrapping to generate over 3000 synthetic dataset fits (see methods for details). Where mutations or insertions have been introduced, we allow the parameters expected to be affected by the mutation to vary locally for the corresponding data set. Moreover, six mutants can be fit with fewer local parameters than were utilized in the fit, as the values for some of these locally fit parameters remain close to the globally fit value (within 10%), as highlighted in **Table 1** (green).

We are able to obtain a remarkably good fit for our entire dataset with the aforementioned considerations. **Figure 7C** shows the results of the best obtained fit for 'wild type' PhoQ (Y60C) sensor-crosslinking and autokinase activity. Since the wildtype data is fit entirely globally, it represents the most stringent test for the performance of our model overall, and qualitatively shows good agreement between model fit and experimental data. The values of the eight global parameters corresponding to this wild type fit are shown in **Figure 7D**, alongside two metrics of fit quality. The first metric is a bootstrapped confidence interval, with the frequency histogram of resulting fit values shown in the top panels. The second metric is a parameter sweep analysis in which the global sum of residuals is evaluated as the value of the indicated parameter is allowed to vary while all other parameters are held fixed. Five of our global parameters, K_{dOFF}, K_{dON},

416 K_{Sen}, K_{HAMP} and α_1 show excellent convergence to the 'best fit' value, with well-defined minima
417 in the sum of residuals as we explore parameter value. Three parameters, K_{AK}, S and α_2 show
418 strong signs of covariability, and wider confidence intervals. In the fully activated state, the
419 observed signal is defined by the product of the scaling factor, S, and the fraction of the protein
420 in the 'kinase-on' state (approximately $S*K_{AK}$). This product is well-defined and converges to a
421 value of ≈ 1.02. However, as K_{AK} is lowered below this value, S increases in parallel to maintain
422 a constant value for the product of $S*K_{AK}$. In **Figure 7-figure supplement 1**, we show that when
423 the values of S are restrained, the values of K_{AK} are also restrained, and vice versa. Nevertheless,
424 we can place a mechanistically meaningful upper limit on K_{AK}, of approximately 0.1. Similarly,
425 we can place an upper limit on the value of 0.1 for α_2, which represents the negatively
426 cooperative coupling of K_{AK} to the parameters defining the other domains. These uncertainties
427 do not affect any of our conclusions below, which depend on presence of strong versus weak and
428 negative versus positive coupling.

429 One feature that was somewhat surprising was that K_{AK} is actually unfavorable towards
430 forming the 'kinase-on' versus 'kinase-off' states ($K_{AK} < 1$), even at limiting low concentrations
431 of Mg^{2+}. This indicates that the observed activity for the WT protein is less than what is observed
432 for some of the mutants, and what might be observed in a hypothetical state in which the
433 autokinase is unfettered by connections to HAMP and the membrane. Although unexpected, this
434 finding is consistent with a large body of data (51–53), and has been observed in PhoQ with
435 antimicrobial peptide stimulation (54). Thus, in ligand-responsive HKs, evolution does not drive
436 towards maximal activity which might lead to wasteful and toxic transcription, but instead a
437 finely tuned value that is titrated to the degree of transcription required for function.

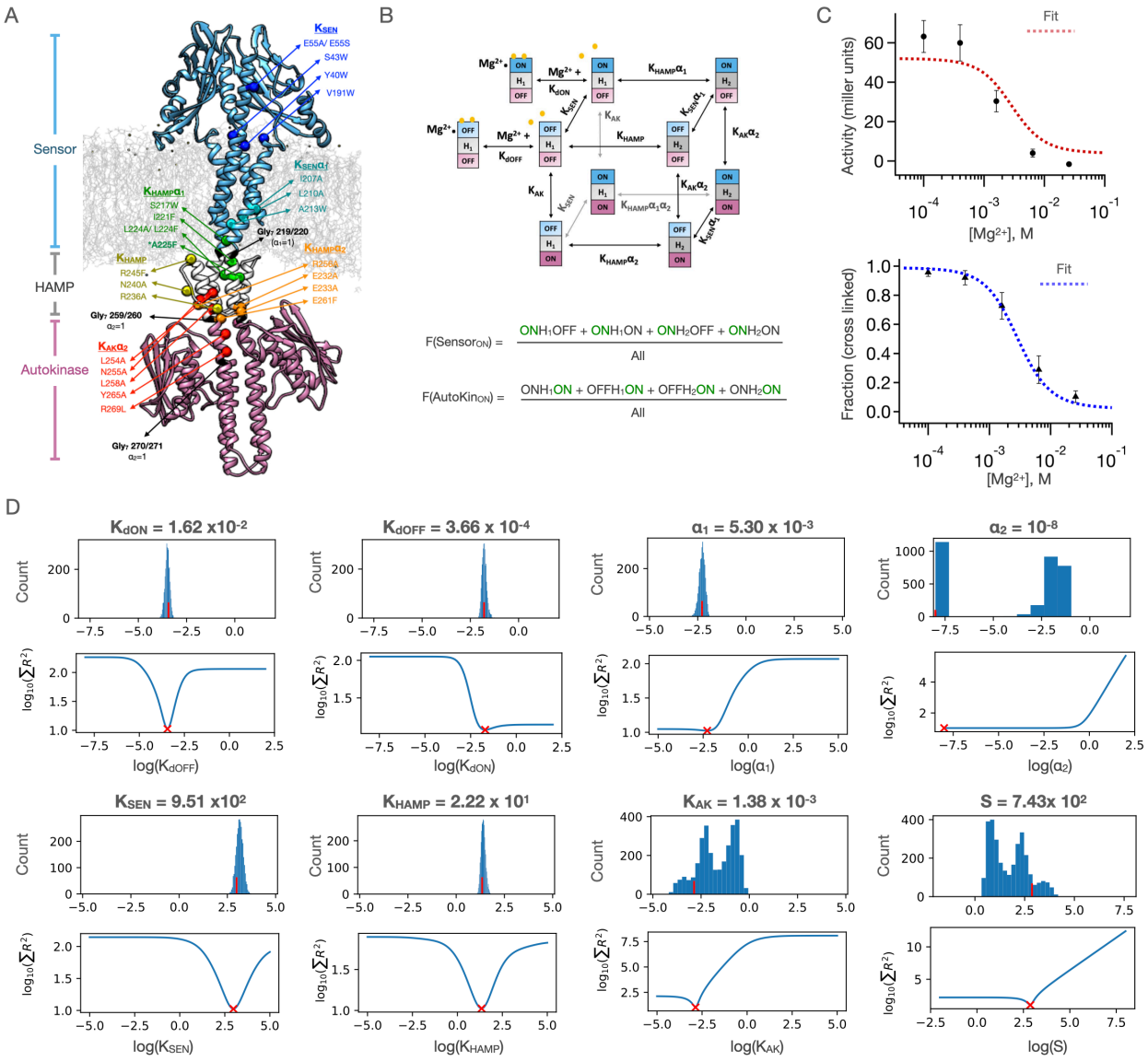

Figure 7 – Results of 3 domain 2-state allosteric model fit of PhoQ activity. **A)** homology model of full length PhoQ showing positions of point mutations and Gly$_7$ insertions used in study. Colored spheres represent the location of the C$_\beta$ sidechain carbon, and are color coded by the identity of local parameters varied. **B)** 3-domain 2-state allosteric model used for fitting (see also **Figure 6A**) **C)** Fits to the [Mg^{2+}] dependent activity (top) and sensor crosslinking (bottom) for 'wild type' Y60C PhoQ are shown. Error bars correspond to ± SD for n=9 biological replicates. **D)** Bootstrapped confidence intervals (top) and residual sweep analyses (bottom) are shown for all 8 global parameters. The value of the fit is indicated with red (x) and (|) marks. The confidence intervals of parameters S, K_{AK} and α_2 are further parsed in **Figure 7-figure supplement 1**.

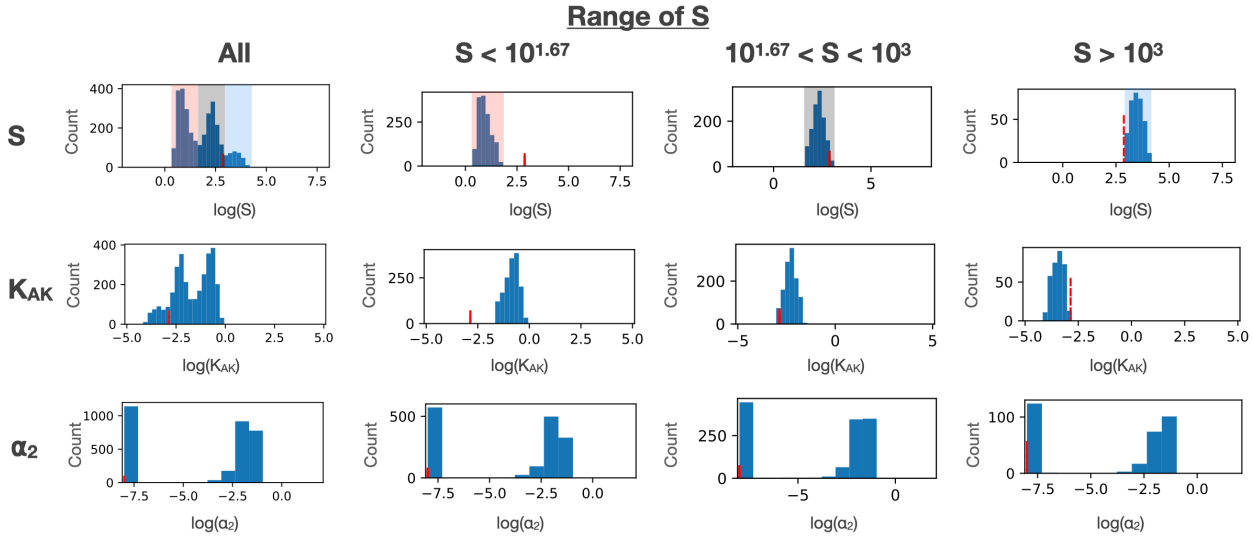

Figure 7-figure supplement 1 – Effect of constraining S and K_{AK}. The confidence intervals for K_{AK} and α_2 parameters are shown as a function of different ranges of S values. S and K_{AK} show strong correlation.

Application of the 3-domain model to a set of mutants illustrates how substitutions distant from active sites modulate signal strength and ligand sensitivity.

The values of the parameters provide a detailed view of the energy landscape of PhoQ, in the 'kinase-on' and 'kinase-off' state – and how it is modulated by binding to Mg^{2+} and mutations. The parameters are consistent with our earlier observations that the HAMP is a significant modulator of the intrinsic equilibria of the sensor and autokinase domains. At high Mg^{2+} concentrations, PhoQ is in a 'sensor-off' and 'autokinase-off' state. With respect to this reference 'kinase-off' state, the HAMP domain has a thermodynamically favored signaling state, '$HAMP_2$', with a fit equilibrium value of $K_{HAMP} = 22$. This favored state of the HAMP is more strongly coupled to these 'kinase-off' states and serves to dampen the otherwise favorable transitions of both the sensor and autokinase domains to the 'kinase-on' conformation. The sensor's propensity to switch to a 'sensor-on' state is reduced from a highly preferred equilibrium $K_{Sen} = 9.51 \times 10^2$, to a modest downhill equilibrium of $\alpha_1 K_{Sen} = 5.0$ when the HAMP is in this $HAMP_2$ state. This latter equilibrium is weak enough to be overcome by Mg^{2+} binding, and the 'sensor-off' state is further stabilized with more ligand binding. The '$HAMP_2$' state that

is preferred in this state is also strongly coupled to the 'kinase-off' state of the autokinase, reducing the propensity of the autokinase to switch to the 'kinase-on' state from $S.K_{AK} = 1.0$ to $\alpha_2.S.K_{AK} \leq 10^{-3}$. Thus, the $HAMP_2$ state behaves as a negative modulator of the intrinsic propensities of the sensor and autokinase. At high enough $[Mg^{2+}]$, the entire population ensemble is predominantly in the $sensor_{OFF}$-$HAMP_2$-$Autokinase_{OFF}$ state.

In the absence of ligand, the sensor's modest downhill equilibrium to the 'kinase-on' state is strongly tied to a switch of the HAMP from '$HAMP_2$' to '$HAMP_1$', with an equilibrium $= 1/(\alpha_1 K_{HAMP}) = 25$. The $HAMP_1$ state is weakly coupled to the autokinase, which allows the autokinase to sample both kinase-off and kinase-on state, with an effective equilibrium of $S.K_{AK} = 1.02$. This allows for the partial decoupling of the sensor and the autokinase at low Mg^{2+} concentrations observed in wild type PhoQ with the population ensemble composed of both $sensor_{ON}$-$HAMP_1$-$Autokinase_{ON}$ and $sensor_{ON}$-$HAMP_1$-$Autokianse_{OFF}$ states. Because the $HAMP_1$ state is weakly coupled to both adjacent domains, the equilibria constants K_{Sen} and K_{AK} are close to the intrinsic equilibria of these domains when uncoupled form the HAMP altogether. In other words, $K_{Sen} = 9.5 \times 10^2$ reflects the high propensity of the sensor to switch to the 'sensor-on' state when uncoupled from the HAMP, and $S.K_{AK} = 1.0$ reflects the propensity of the autokinase to have as high an activity as full length PhoQ at low $[Mg^{2+}]$, as shown earlier with Gly_7 disconnections in **Figure 4**.

The parameters for individual mutants show how amino acid substitutions alter the energy landscape and how these changes in turn alter the phenotype. Before discussing the effects of substitutions, however, it is important to address the overall quality of the fit over the full ensemble of mutants. **Figure 8** shows the results of fits for our mutations and Gly_7 insertions, and the locally varied parameters. The corresponding fit values are listed in **Table 1**,

and confidence intervals and parameter sensitivity analyses are shown in **Figure 8-figure supplement 1**. We obtain fits within experimental error for the [Mg^{2+}]-dependent transcriptional activity of our entire mutant data set. Thus, the model works well for all functional mutants. The only deviations lie in the crosslinking data for non-functional mutants that are decoupled in the transcriptional assay (**Figure 8-figure supplement 2**). One such set of mutants (I221F, L224A and A225F) have substitutions at the C-terminal end of the second TM helix. While the midpoint and lower limit were well described by the model, the experimentally observed extent of crosslinking reaches an upper limit of 65% to 80% crosslinking at low Mg^{2+}, less than the predicted value near 100%. Given the location of the substitutions near the membrane interface, it is possible that a portion of the protein is not fully inserted and hence the samples used for western analysis might have been contaminated by cytoplasmically localized, and not yet membrane-inserted protein, which would be expected to remain un-crosslinked. There are also two mutants localized near the interface between the HAMP and the autokinase domains where the mid-point is poorly fit (L254A, L258A), potentially owing to our choices of parameters to locally float for these mutants (**Figure 8-figure supplement 2D-E**) as discussed in methods. Significantly better fits were obtained by altering the parameters varied for these mutants from K_{HAMP} and α_2 to K_{AK} and α_2. Thus, these residues may be involved in the underlying equilibrium of the autokinase domain itself due to their proximity to the "S-helix" that connects the HAMP to the autokinase domain. Finally, double mutants are not fit well, especially when the two sites of mutation are in close proximity (S217W + HAMP Gly_7, N255A + HAMP Gly_7, Y265A + Sensor Gly_7, **Figure 8-figure supplement 2F-H**). This is likely because the thermodynamic effects of double mutants are often non-additive in structurally and sequentially proximal positions that interact directly. Additionally, while we observe relatively invariant expression of almost all

variants (as seen in the western analysis used to quantify crosslinking), some variants, particularly double mutants required slight induction of expression with 10 μM IPTG for observable levels of membrane-inserted PhoQ by western-blotting (see methods). In summary, the crosslinking and transcriptional activity data are very well fit for the entire set up mutants, except for a fraction of the nonfunctional mutants in which Mg^{2+} binding and transcription were significantly decoupled. Even for these mutants, however, there is a qualitative fit to the data, and likely reasons for the deviation.

Our results illustrate the coupling of sequence and energetic landscapes in response to single-site substitutions. Although we chose a collection of mutants that were not involved in Mg^{2+} binding and catalysis, we observed a large range of effects on the transcriptional response of the mutants, including an inverse response in E232A and Gly_7 270/271 insertion. The advantage of the current analysis is that it shows how these mutations are able to alter the energetics of individual domains, and their coupling to adjacent domains. As an organism evolves to match its environment, its sensory systems need to adjust to the ligand-sensitivity (midpoint of the dose-response curve), the magnitude of the increase in the response (in this case, the (activity in the absence of Mg^{2+}/activity in presence of Mg^{2+}) and the basal activity (in the presence of saturating Mg^{2+}). We consider these features separately.

In a well-coupled system such as WT PhoQ, the midpoint can be modulated by point mutants anywhere along the signal transduction pathway between the sensor and the autokinase. The only requirement is that the substitution has an effect on the internal equilibrium constant for the kinase-promoting versus the phosphatase-promoting conformations of the domain that houses the mutant. So long as the domains are tightly coupled, then an n-fold change in the internal equilibrium will translate to an n-fold change in the midpoint of the overall dose-response curve.

Moreover, as the couplings α_1 and α_2 become less strong, the magnitude of the shift in the dose response curve is decreased. Thus, it is not necessary to change the binding interactions with the metal ions to affect changes in the ligand sensitivity of the system which provides the system a wealth of opportunities to tune sensitivity.

The fractional change in the kinase activity that can be achieved upon saturation of the ligand-binding sites is a second factor, which ranges with the requirements of a system. For example, the change in transcriptional response in PhoQ is modest, reaching about a factor of 5 to 20-fold change, while other two-component systems such as VirA have a dynamic range as large as 10^5 (52,55–57). For simple systems that respond to a single ligand, the maximal response is defined by the ratio of the intrinsic affinity of the sensor for the 'kinase-on' versus 'kinase-off' conformations (K_{dON}/K_{dOFF}). Mutations that decrease the coupling attenuate the maximal response, and the system becomes decoupled when α_1 or α_2 reaches 1. The maximal response in absolute terms is another factor, which depends on the kinetic efficiency of the underlying autokinase domains. When untethered from the membrane, some autokinase domains show large increases activity, so the role of the remainder of the protein can be seen as a negative regulation. Indeed, we find that K_{AK} is significantly less than 1, and this value can be positively modulated by some mutants that reach transcriptional levels somewhat greater than WT for PhoQ. In summary, there is a diversity of mechanisms that nature can call upon to alter the activity of HKs, as illustrated in a relatively small sampling of the 35 mutants studied here.

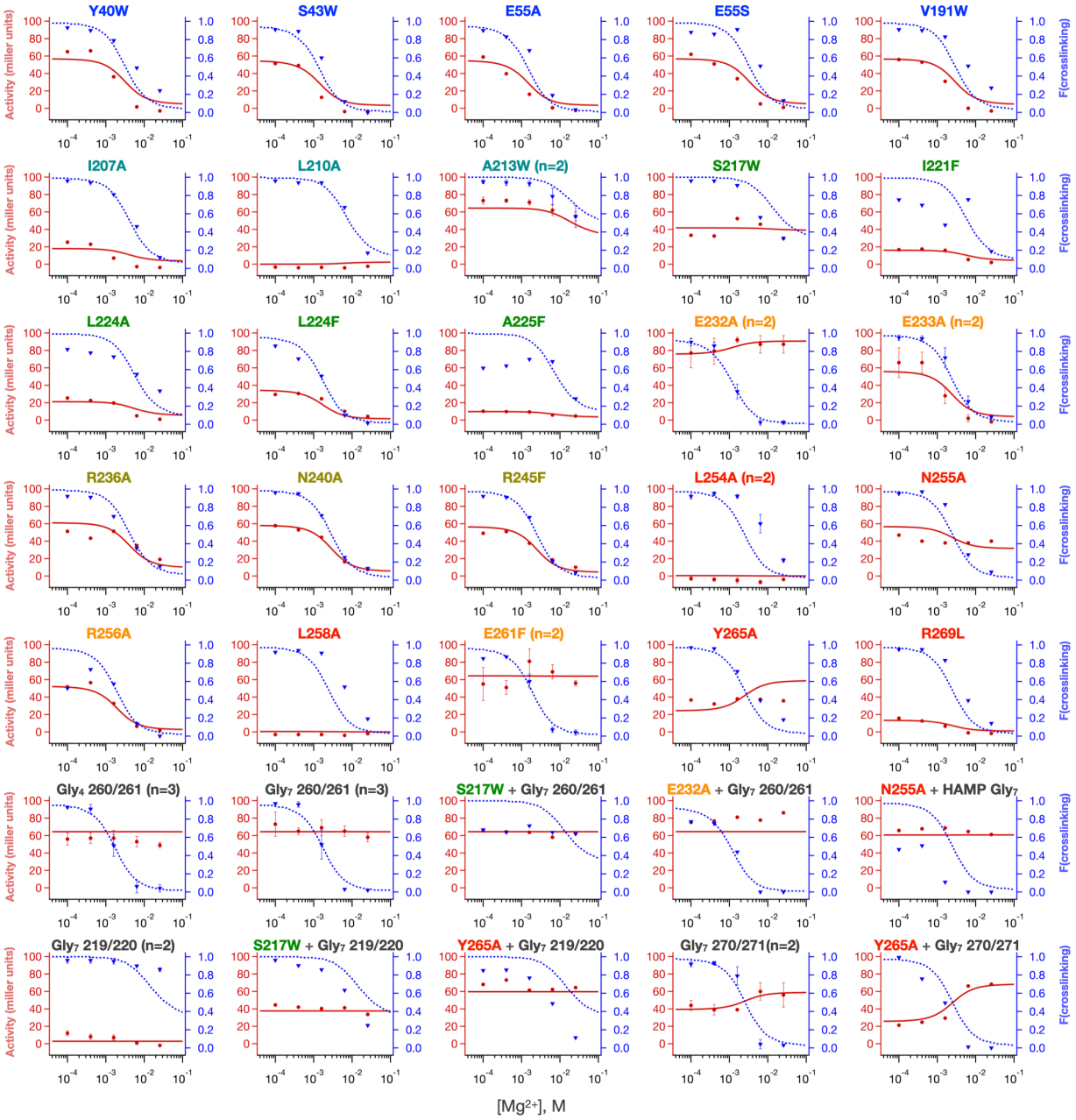

Figure 8 – Local fits of sensor crosslinking and kinase activity for 35 PhoQ mutations. Fits to activity (red line, closed circles) and sensor crosslinking (blue dashed line, triangles) are shown for the entire PhoQ dataset. The identity of locally varied parameters is listed in **Figure 7A** and **Tables 1** and **2**. Confidence intervals and residual sweep analyses are presented in **Figure 8-figure supplement 1**. Poor fits are highlighted in **Figure 8-figure supplement 2**.

Figure 8-figure supplement 1 – Bootstrapped confidence intervals and residual sweep analyses for PhoQ mutant fits. Histograms from 3061 convergent fits of simulated datasets for each local variable are shown in top panels. Residual sweeps in which the sum of residuals of the global fit is plotted as a function of indicated parameter being varied locally is shown in the bottom panels. Values of parameter fits are shown with red (x) and (|) marks.

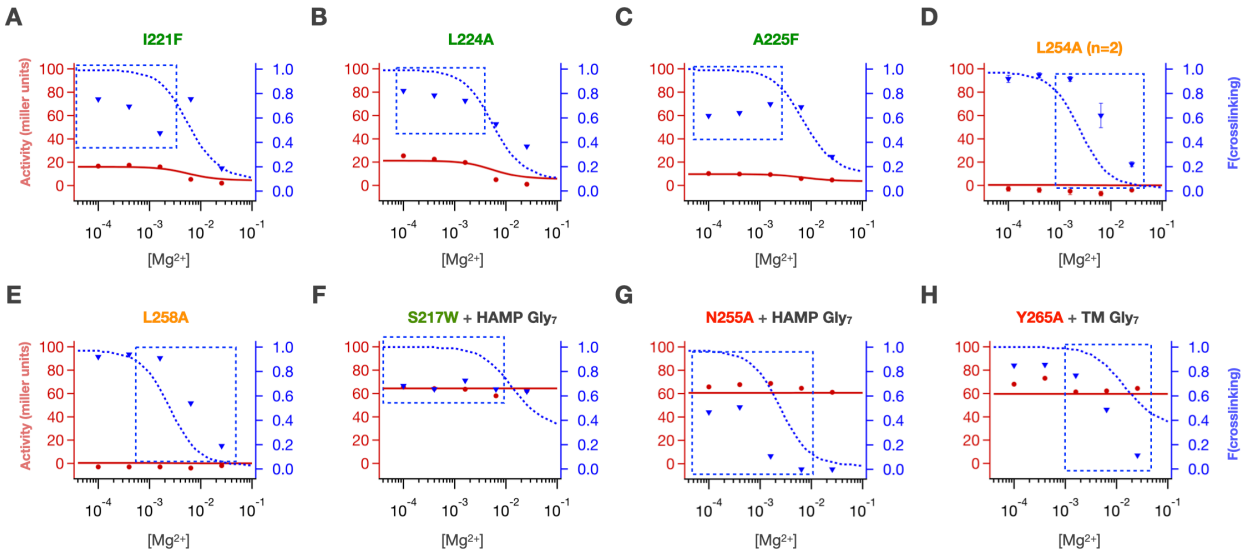

Figure 8-figure supplement 2. Poor fits were obtained for crosslinking at low [Mg^{2+}] for **(A)** I221F, **(B)** L224A and **(C)** A225F. Poor midpoints of crosslinking transitions were fit for **(D)** L254A and **(E)** L258A. Some combinations of mutations had poor crosslinking fits **(F)** S217W + HAMP Gly_7, **(G)** N255A + HAMP Gly_7 and activity fits **(H)** Y265A + sensor Gly_7

Discussion

It has been appreciated for several decades that the effector domains of multi-domain signaling proteins can produce responses that are either more potentiated or diminished relative to the change in state of sensory domains that drive these responses. S J Edelstein and J P Changeux in seminal work coined the terms “hyper-responsive” and “hypo-responsive” to define this uncoupled behavior between domains, which has since been examined in other classes of multi-domain signaling proteins such as GPCRs (58). In this work, we examine the coupling behavior between the sensor and effector domains of transmembrane bacterial sensor histidine kinases and possible roles of modularly inserted signal transduction domains in optimizing this coupling behavior using a model gram negative HK, PhoQ. We find that the intervening HAMP signal transduction domain is necessary to assemble an overall bistable histidine kinase from Mg^{2+}-sensor and autokinase-effector domains that are too biased to one signaling state (‘kinase on’ state). This is accomplished by strongly coupling the thermodynamically preferred state of the HAMP to the disfavored ‘kinase off’ signaling states of sensor and autokinase, ameliorating

585 these otherwise strong equilibria such that the overall assembly is bistable and significantly
586 modulated by ligand binding. Thus, the HAMP does more than transmit the response; it instead
587 serves to tune the ligand-sensitivity amplitude of the response.

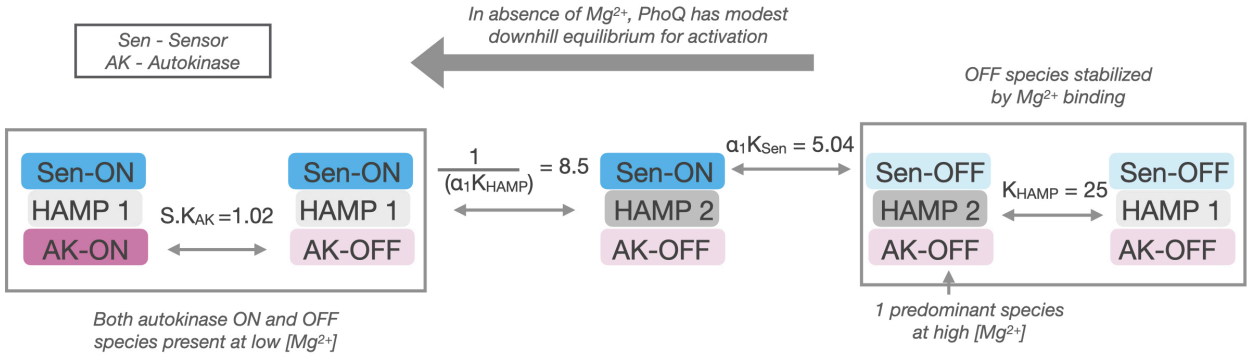

588
589 **Figure 9 – Allosteric pathway for PhoQ activation.** In the absence of Mg^{2+}, PhoQ has a moderate downhill
590 equilibrium to a mixture of active states. Mg^{2+} binding is sufficient for overpowering this equilibrium and stabilizing
591 the 'kinase-off' state, resulting in a predominantly Sensor-off/HAMP2/Autokinase-off population.
592
593 Evolutionarily, the insertion of signal transduction domains in HKs could allow for the
594 facile modulation of the intrinsic equilibria of sensor and effector domains and their coupling
595 behavior, which may be more difficult to alter through the direct mutation of these domains
596 themselves. The sequence and subsequent structures of sensors and autokinase domains are
597 subject to many evolutionary constraints, be it the specificity and affinity for ligands in sensor
598 domains, the specificity for membrane homodimerization of HKs (59), or the cognate specificity
599 for response regulator (13,60–63) and the ability to inhabit and switch between the various
600 conformations required for a full catalytic cycle in the autokinase domain (15). Furthermore,
601 most two-component systems feature multiple accessory protein components involved in
602 sensing, feedback regulation and cross-talk with other signaling systems, which add evolutionary
603 constraints to these domains (64). In the closely related class of chemotaxis proteins, the
604 analogous transmembrane protein is also subject to extensive covalent modifications that
605 modulate activity. When all these evolutionary activity and specificity considerations are met,
606 the resulting domain may not be ideally bi-stable in isolation. Indeed, in PhoQ, we find that both

607 sensor and autokinase highly prefer the 'kinase-on' state, and therefore cannot be allosterically
608 connected to make an overall bistable protein capable of being converted to the 'kinase-off' state
609 by Mg^{2+} binding. The presence of one or more signal transduction domains allows for 2
610 advantageous considerations for producing and finetuning overall HK bistability; the
611 thermodynamic stability of the signal transduction domain can be used to preferentially stabilize
612 or destabilize a given signaling state of sensors or autokinases indirectly through allosteric
613 coupling, and the strength and even direction of coupling can be easily modulated through
614 mutations at the domain junction, rather than mutations that may alter the core functions of the
615 sensor/autokinase themselves.

616 The latter phenomenon is especially potent in the context of alpha-helical coiled-coil
617 connections between domains of HKs, in which a drastic change in coupling or thermodynamic
618 stability can be caused by minor sequence insertions, deletions and alterations due to the highly
619 regular and cooperative nature of coiled-coil stabilizing interfaces. We have shown that the
620 insertion of a stretch of glycine residues is sufficient to completely uncouple domains. On the
621 other extreme, a well folded coiled coil junction can create strong allosteric coupling due to the
622 cooperative folding and stability of such a motif. A range of stabilities can be achieved by
623 various means, including the insertion or deletion of one or more residues to disrupt the
624 canonical heptad pattern of hydrophobic residues of the dimeric core of the protein, as is often
625 observed in the conserved S-helix motif, which connects HAMP to autokinase domains in HKs
626 (65). Schmidt *et. al.* (66) showed that crystal structures of cytoplasmic domains in different
627 conformations accommodate the structural deviations of these S-Helix sequence insertions by
628 diffusing the strain over different lengths of the proximal alpha-helical core. These different
629 "accommodation lengths" could be analogous to the different strengths of allosteric coupling

630 depending on the signaling states of the adjacent domains in our equilibrium signaling model.
631 We also find conservation of glycine motifs and helix-disrupting proline residues in the juxta-
632 membrane regions of chemotaxis proteins and HKs respectively (51,67,68), which hint at the
633 significant modulation of allosteric coupling strength by the alteration of helical and coiled-coil
634 geometries. In some systems, domains are even segregated to entirely different proteins, in which
635 case the strength of the protein-protein interaction between components can be altered to vary
636 allosteric coupling. These are all evolutionarily accessible solutions to fine-tune the function of a
637 histidine kinase.

638 Finally, this evolutionary argument may also explain the lack of a parsimonious structural
639 mechanism for signal transduction, even in HKs with a specific domain architecture. Although
640 this problem is largely exacerbated by the dearth of multi-domain structures of HKs in various
641 signaling conformation, several signaling hypotheses have been put forward regarding the
642 structural mechanism for signal transduction in HKs, particularly in HAMP domains. These
643 include the gear-box mechanism (AF1503, Aer2 multi-HAMP)(69), Piston mechanism (Tar)
644 (70,71), Scissoring mechanism (Tar, BT4663, PhoQ) (72–74), Orthogonal displacement
645 mechanism (HAMP tandems, Tar) (75–77) and the dynamic HAMP mechanism (Adenylate
646 cyclase HAMP) (78–80). A recently elucidated set of structures of the sensor, TM and signal
647 transduction domains of NarQ remains the only representative of a multidomain transmembrane
648 structure of an HK containing a signal transduction domain, and again shows a rigid-body
649 bending transition of the HAMP domain about the conserved N-term Proline between apo- and
650 holo-states of the sensor(81).

651 It may be that signal transduction mechanisms in HKs are as varied as their modular
652 architecture, and many structural transitions could account for the underlying concern in

653 signaling, which is the allosteric modulation of multi-state equilibria of adjacent domains in
654 response to structural transitions caused by a sensory event. Indeed, the only requirement for
655 signal transduction is a series of domains with two states that either favor or disfavor the kinase
656 state, and a means to transmit the information between the states. Helical connections between
657 domains provide efficiently coupling, but the conformational changes within the domain need
658 not be obligatorily the same for different domains. Additionally coupling can involve tertiary
659 contacts, which can be used in conjunction with or instead of helical connections. Interestingly,
660 the observation that PhoQ has a weakly HAMP-coupled 'kinase-on' state and a strongly HAMP-
661 coupled 'kinase-off' state has been posited before, albeit in the context of a hypothesized tertiary
662 contact between the membrane-distal portion of HAMP helix-1 and a loop in the autokinase
663 domain (54). The idea that autokinase domains intrinsically have high-kinase activity and are
664 subsequently inhibited by strong coupling to up-stream domains and the further stabilization of
665 these inhibitory conformations by ligand-binding warrants examination as a generalizable
666 signaling mechanism for histidine kinases.

667 **Materials and Methods:**

668 **Materials:**

669 BW25113 and HK knockout strains were obtained from the Keio collection.

670 TIM206 (*E. coli* Δ*phoQ*, p*mgrB*::LacZ) was obtained from Tim Mayashiro (Goulian lab)

671 pTrc99a (GenBank # M22744)

672 pSEVA311 (GenBank# JX560331) was developed by the de Lorenzo lab and was a gift from the
673 European Standard Vector Architecture consortium.

674 Brilacidin was a gift from Polymedix Inc.

675 N-ethylmaleimide (NEM, Sigma)

Tris-Acetate gels (Thermofisher Scientific)

Anti-PentaHis antibody (Thermofisher Scientific)

Methods:

Cloning: PhoQ mutants were cloned into the pTrc99a plasmid MCS by restriction cloning. Point mutations were made by quick-change mutagenesis and confirmed by sanger sequencing. Hybrid HK-gene reporter plasmids were built in pTrc99a plasmid by introducing a c-terminally 6x His-tagged HK construct into the IPTG inducible MCS, and the mCherry reporter sequence downstream by Gibson cloning. Sequences of reporters are available in supplementary methods. Gly_7 disconnections and point mutations were introduced by a blunt-end ligation strategy and confirmed by sanger sequencing.

Growth of PhoQ constructs: For each biological replicate, an isolated colony of TIM206 (genotype: Δ*phoQ*, p*mgrB*::LacZ) containing various pTrc99a-*phoQ* constructs was grown overnight at 37 °C in MOPS minimal media + 50 µg/mL AMP and 1 mM $MgSO_4$. These overnight cultures were then diluted 50x into 1 mL MOPS media + 50 µg/mL AMP and 1 mM $MgSO_4$ and grown at 37°C for 2 hours. These cultures were further diluted 500X into 30 mL MOPS minimal media + 50 µg/mL AMP containing 0.1, 0.4, 1.6, 6.4 and 25.6 mM $MgSO_4$, and grown for at least 5 hours such that the density of the culture reaches log-phase (OD_{600} = 0.2 – 0.8). 500 µL of culture is removed for evaluating beta galactosidase activity, while the remaining culture is used for western analysis. Two constructs (A225F, Y265A Gly_7 260/261) required induction with 10 µM IPTG during growth for observable levels of membrane inserted PhoQ by western blot.

Beta galactosidase activity: 500 µL of PhoQ culture was combined with 500 µL of 1x Z-buffer + 40 mM beta-mercaptoethanol, 25 µL of 0.1% SDS in water, and 50 µL of chloroform in a

699 glass culture tube and vortexed for complete lysis. The lysate was then prewarmed to 37°C in a
700 standing incubator before addition of ONPG substrate. 0.25 mL of prewarmed 4 mg/mL ONPG
701 in 1x Z-buffer + bMe was added to the lysate to initiate hydrolysis, which was then quenched
702 with the addition of 500 µL of 1M Na_2CO_3 after variable incubation periods. The quenched
703 hydrolysis was then centrifuged to remove any cell debris, and absorbance at 420 nm and 550
704 nm was measured in triplicate using a Biotek synergy2 plate-reader with pathlength correction.
705 Miller units were calculated as follows:
706 Miller units = $1000*(OD_{420} - 1.75*OD_{550})/(OD_{600}*\text{dilution factor}*\text{incubation time in min})$
707 **Membrane fraction isolation:** 30 mL of PhoQ culture was centrifuged at 4°C for 20 minutes to
708 collect a cell-pellet. This cell-pellet was immediately frozen in liquid nitrogen and stored at -
709 80°C until analysis. Frozen pellets were first thawed, suspended and incubated on ice with 500
710 µg/mL N-Ethylmaleimide (NEM) and 1 mg/mL lysozyme in 50 mM TRIS buffer, pH 8, for 1
711 hour. Cells were then lysed by 30 seconds of tip-sonication. Lysed cells were then centrifuged at
712 16000xg for 10 minutes to remove cell debris. Membrane was isolated from the supernatant by
713 further centrifugation at 90,000xg for 10 minutes. Membrane pellets were then resuspended in
714 1X LDS loading buffer containing 8M Urea and 500 mM NEM, boiled at 95°C for 10 minutes
715 and analyzed by western blot.
716 **Monomer and dimer quantification by western blot:** Samples were first separated on 7%
717 TRIS-SDS gels by electrophoresis at 200V for 70 min, and then transferred onto nitrocellulose
718 membranes by dry transfer (iBlot2). Membranes were then blocked using 1% BSA in TBS-t
719 buffer (20 mM Tris, 2.5 mM EDTA, 150 mM NaCl, 0.1% Tween-20), probed using an anti-
720 pentaHis HRP antibody, and visualized using luminescent ECL substrate on a BioRad imager.

721 Bands corresponding to PhoQ monomer and dimer were quantified using Image-J software to
722 yield a crosslinking efficiency between 0 and 1.

723 **Measuring activity of CpxA, BaeS:** HK constructs were cloned into the MCS of pTrc99a
724 plasmid, and the associated fluorescent reporter gene was cloned downstream. For the CpxA
725 reporter plasmid, the response regulator CpxR, was also cloned into the MCS and transformed
726 into AFS51 strain (Δ*cpxA*Δ*pta*::Kan p*cpxP*::GFP) by heat shock transformation. For BaeS, the
727 response regulator BaeR, was cloned into an additional plasmid, pSEVA331 under an IPTG
728 inducible promoter and both plasmids were transformed into a Δ*baeS*Δ*cpxA* double KO strain by
729 heat shock transformation. Cultures were started by diluting overnights 200-500 folds into fresh
730 LB + 50 µg/mL AMP media and allowed to grow to mid-log phase (OD_{600} = 0.4 – 0.6) before
731 analysis by flow cytometry. The responsiveness of *cpxP* reporter was confirmed by treating log-
732 phase cultures with 2 µg/mL Brilacidin for 1.5 hours before analysis. Expression of HKs was
733 confirmed by western analysis using the c-terminal 6x His-tag for quantification.

734 **Flow cytometry:** LB cultures at mid-log phase were diluted 20x into 1x PBS buffer and 20,000
735 cells gated by forward and side-scatter were evaluated for GFP fluorescence (p*cpxP*::GFP; Ex.
736 488 nm, Em. 515 nm) or mCherry fluorescence (p*spy*::mCherry, Ex. 488 nm, Em. 620 nm) per
737 sample on a BD FACS caliber instrument. Sample average fluorescence and standard error were
738 determined by standard analysis using Flo-Jo software.

739 **Data Fitting:** For data fitting, only data-sets in which kinase activity and sensor crosslinking
740 have been determined simultaneously from the same samples at all 5 concentrations of Mg^{2+}
741 were included in analysis. This resulted in Kinase active and sensor crosslinking competent
742 states are partitioned to generate expressions dependent on [Mg^{2+}] as the lone variable as shown
743 below. The parameters are then fit globally across all datasets, except for those accounting for

the perturbation of a mutant/ Gly_7 disconnection, which are fit locally. Locally fit parameters are kept identical between replicates or additive mutations.

$$F(Sensor_{ON}) = \frac{Sen_{ON}HAMP_1AK_{OFF} + Sen_{ON}HAMP_1AK_{ON} + Sen_{ON}HAMP_2AK_{OFF} + Sen_{ON}HAMP_2AK_{ON}}{All}$$

$$= \frac{\left(1+\frac{[Mg^{2+}]}{K_{dON}}\right)^2 * (K_{sen} + K_{Sen}K_{AK} + \alpha_1 K_{Sen}K_{HAMP} + \alpha_1\alpha_2 K_{Sen}K_{HAMP}K_{AK})}{\left(1+\frac{[Mg^{2+}]}{K_{dON}}\right)^2 * (K_{Sen} + K_{sen}K_{AK} + \alpha_1 K_{Sen}K_{HAMP} + \alpha_1\alpha_2 K_{Sen}K_{HAMP}K_{AK}) + \left(1+\frac{[Mg^{2+}]}{K_{dOFF}}\right)^2 * (1 + K_{AK} + K_{HAMP} + \alpha_2 K_{HAMP}K_{AK})}$$

$$F(AutoKin_{ON}) = \frac{Sen_{OFF}HAMP_1AK_{ON} + Sen_{OFF}HAMP_2AK_{ON} + Sen_{ON}HAMP_1AK_{ON} + Sen_{ON}HAMP_2AK_{ON}}{All}$$

$$= \frac{\left(1+\frac{[Mg^{2+}]}{K_{dOFF}}\right)^2 * (K_{AK} + \alpha_2 K_{HAMP}K_{AK}) + \left(1+\frac{[Mg^{2+}]}{K_{dON}}\right)^2 * (K_{sen}K_{AK} + \alpha_1\alpha_2 K_{Sen}K_{HAMP}K_{AK})}{\left(1+\frac{[Mg^{2+}]}{K_{dON}}\right)^2 * (K_{Sen} + K_{sen}K_{AK} + \alpha_1 K_{Sen}K_{HAMP} + \alpha_1\alpha_2 K_{Sen}K_{HAMP}K_{AK}) + \left(1+\frac{[Mg^{2+}]}{K_{dOFF}}\right)^2 * (1 + K_{AK} + K_{HAMP} + \alpha_2 K_{HAMP}K_{AK})}$$

To ensure equal weights in global fitting, the activity data was scaled by a factor of q = (mean of activity data) / (mean of %crosslink data). The crosslinking data and refactored activity data (Activity / q) were then globally fit to a 3-state allosteric model. Each of 56 datasets (including replicates) was fit by a combination of global and local parameters, described in **Table 2**. Global parameters were shared between replicate datasets as well as datasets of mutations that were functionally similar. A total of 62 parameters (global and local, **Table 2**) were optimized using the python code found in the supplement (phoq_fit_local_global.py), from many rounds of fitting starting with random initial conditions (125,000 independent fits). Error analysis of the best-fit parameters (minimized sum of squares of residuals) was performed through bootstrapping of residuals with replacement to calculate confidence intervals, as well as residual sweep analyses (see below). To create synthetic bootstrapped datasets, we chose residuals at random with replacement and added these residuals to the activity and %crosslink values from the optimum fit. For each synthetic dataset, parameters were re-optimized, starting from initial values taken

from the optimum fit. Out of 10,000 generated datasets 3061 fits were determined to have converged. The optimization process was considered converged when the cost function F did not change considerably (dF < ftol * F, with ftol = 1e-8, i.e., convergence criterion 2 from Scipy least_squares). Histograms of these bootstrapped parameter values show the spread in possible values due to errors in the fit (**Figure 7c** and **Figure 8 figure supplement 1**). Analysis of the bootstrapped parameter distributions showed correlations between the globally fit parameters S and K_{AK} (**Fig. 7 figure supplement 1**).

We also performed a residual sweep analysis to assess the quality of the fit in response to changes in a single parameter value, with all other parameters held fixed. For residual sweep analysis, all but one of the parameters were fixed to their optimum values, and the variable under analysis was swept across its allowed numerical range, after which the sum of squares of residuals was calculated. The sum of squares was then plotted as a function of the parameter's numerical value (**Figure 7C** and **Figure 8 figure supplement 1**). Code to reproduce the fits and plots is given in the comment section at the bottom of the supplement python scripts (phoq_fit_local_global.py, phoq_fit_local_global_ipython.py, and phoq_fit_ci_local_global.py). Scripts to run the fitting on the UCSF Wynton High Performance Computing cluster can also be found in the supplement (phoq_fit.job and phoq_fit_ci.job).

Choice of locally varied parameters: mutations contained entirely within a given domain are allowed to vary the intrinsic equilibrium of that domain only. Mutations within 1 heptad of a domain-domain junction (219/220 for sensor/HAMP, 260/261 for HAMP/autokinase) are also allowed to vary the equilibrium constant of the domain they reside in, as well as the coupling constant between the two domains. Exceptions to this rule include A225F, which was additionally allowed to vary the K_{Sen} parameter, along with K_{HAMP} and α_1 parameters which

783 would normally be varied. Given the poor fit to this mutant, we hypothesized that the disruption
784 of inserting a large Phe sidechain in place of an alanine may propagate into the preceding
785 transmembrane region. Similarly, we allowed K_{AK} to float locally for L254A, N255A and
786 L258A, which resulted in better fits as discussed in main text. Finally, α_2 was allowed to float for
787 E231A, and E232A, which have been hypothesized in previous work to directly couple to the
788 autokinase domain via a salt-bridge to an arginine residue in the autokinase (54).
789

790 **Acknowledgements.**

791 **Funding:** We acknowledge research support from a grant from NIH (R35 GM122603).
792

Table 1- List of mutant parameter fits.

Local parameters whose values remained within 10% of the global fit value are highlighted in bold font and green background. Parameters whose value drifted to one end of the explored parameter range are highlighted in italicized font and orange background.

Mutant	K_{Sen}	K_{HAMP}	K_{AK}	α_1	α_2	s	K_{dOFF}	K_{dON}
Y60C	9.5 E +02	2.2 E +01	1.4 E -03	5.3 E -03	*1.0 E -08*	7.4 E +02	3.7 E -04	1.6 E -02
Y60C HAMP 4		4.5 E +01			1.0 E +00			
Y60C HAMP 7					1.0 E +00			
Y60C SH7		**2.1 E +01**	7.7 E -04		1.7 E +00			
Y60C TM7				1.0 E +00				
Y40W	1.4 E +03							
S43W	3.8 E +02							
E55A	4.1 E +02							
E55S	1.5 E +03							
V191W	1.2 E +03							
I207A	6.9 E +02			1.1 E -01				
L210A	3.1 E -03			9.1 E +04				
A213W	4.0 E +04			*1.0 E -05*				
S217W		7.1 E -01		7.6 E -01				
S217W + H7					1.0 E +00			
S217W + TM7				1.0 E +00				
I221F		**2.0 E +01**		1.5 E -01				
L224A		1.6 E +01		1.3 E -01				
L224F		6.8 E +01		1.2 E -02				
A225F	**1.0 E +03**	**2.4 E +01**		2.3 E -01				
E232A		1.1 E +02			1.4 E +00			
E232A + H7					1.0 E +00			
E233A		**2.3 E +01**			*1.0 E -08*			
R236A		8.6 E +00						
N240A		1.7 E +01						
R245F		**2.2 E +01**						
L254A			*1.0 E -05*		*1.0 E -08*			
N255A			**1.3 E -03**		4.9 E -01			
N255A + H7					1.0 E +00			
R256A		3.6 E +01			*1.0 E -08*			
L258A			*1.0 E -05*		*1.0 E -08*			
E261F		3.9 E +01			9.9 E -01			
Y265A			4.1 E -04		3.2 E +00			
Y265A + TM7				1.0 E +00				
Y265A + SH7					3.8 E +00			
R269L			3.3 E -04		*1.0 E -08*			

798 **Table 2 - parameters used in fitting**

Par.	Fit value	lower bound	Upper bound	Fit datasets affected
K_{dON}	1.6 E-02	1.0 E-08	1.0 E+02	ALL
K_{dOFF}	3.7 E-04	1.0 E-08	1.0 E+02	ALL
α_1	5.3 E-03	1.0 E-05	1.0 E+05	Y60C_Gly_7 270/271, Y60C_Gly_7 260/261, Y60C_Gly_4 260/261, Y60C, Y40W, Y265A_Gly_7 270/271, Y265A, V191W, S43W, R269L, R256A, R245F, R236A, N255A Gly7 260/261, N255A, N240A, L258A, L254A, E55S, E55A, E261F, E233A, E232A_Gly_7 260/261, E232A
α_2	1.0 E-08	1.0 E-08	1.0 E+02	Y60C_Gly_7 219/, Y60C, Y40W, V191W, S43W, S217_Gly_7 219/220, S217W, R245F, R236A, N240A, L224F, L224A, L210A, I221F, I207A, E55S, E55A, A225F, A213W
K_{Sen}	9.5 E+02	1.0 E-05	1.0 E+05	Y60C_Gly_7 219/220, Y60C_Gly_7 270/271, Y60C_Gly_7 260/261, Y60C_Gly_4 260/261, Y60C, Y265A_Gly_7 270/271, Y265A, S217W_Gly_7 219/220, S217W_Gly_7 260/261, S217W, R269L, R256A, R245F, R236A, N255A_Gly_7 260/261, N255A, N240A, L258A, L254A, L224F, L224A, L210A, I221F, I207A, E261F, E233A, E232A_Gly_7 260/261, E232A
K_{HAMP}	2.2 E+01	1.0 E-05	1.0 E+05	Y60C_Gly_7 219/220, Y60C, Y40W, Y265A_Gly_7 219/220, Y265A_Gly_7 270/271, Y265A, V191W, S43W, R269L, E55S, E55A, A213W
K_{AK}	1.4 E-03	1.0 E-05	1.0 E+05	Y60C_Gly_7 219/220, Y60C_Gly_7 260/261, Y60C_Gly_4 260/261, Y60C, Y40W, V191W, S43W, S217W_Gly_7 219/220, S217W_Gly_7 260/261, S217W, R256A, R245F, R236A, N255A_Gly_7 260/261, N255A, N240A, L258A, L254A, L224F, L224A, L210A, I221F, I207A, E55S, E55A, E261F, E233A, E232A_Gly_7 260/261, E232A, A225F, A213W
S	7.4 E+02	1.0 E-05	1.0 E+05	ALL
K_{Sen}	1.4 E+03	1.0 E-05	1.0 E+05	Y40W
K_{Sen}	3.8 E+02	1.0 E-05	1.0 E+05	S43W
K_{Sen}	4.1 E+02	1.0 E-05	1.0 E+05	E55A
K_{Sen}	1.5 E+03	1.0 E-05	1.0 E+05	E55S
K_{Sen}	1.2 E+03	1.0 E-05	1.0 E+05	V191W
K_{Sen}	6.9 E+02	1.0 E-05	1.0 E+05	I207A
α_1	1.1 E-01	1.0 E-05	1.0 E+05	I207A
K_{Sen}	3.1 E-03	1.0 E-05	1.0 E+05	L210A
α_1	9.1 E+04	1.0 E-05	1.0 E+05	L210A
α_1	1.0 E-05	1.0 E-05	1.0 E+05	A213W
K_{Sen}	4.0 E+04	1.0 E-05	1.0 E+05	A213W
K_{HAMP}	7.1 E-01	1.0 E-05	1.0 E+05	S217W_Gly_7 219/220, S217W_Gly_7 260/261, S217W
α_1	7.6 E-01	1.0 E-05	1.0 E+05	S217W_Gly_7 260/261, S217W
K_{HAMP}	2.0 E+01	1.0 E-05	1.0 E+05	I221F
α_1	1.5 E-01	1.0 E-05	1.0 E+05	I221F
K_{HAMP}	1.6 E+01	1.0 E-05	1.0 E+05	L224A
α_1	1.3 E-01	1.0 E-05	1.0 E+05	L224A

Par.	Fit value	lower bound	Upper bound	Fit datasets affected
K_{HAMP}	6.8 E+01	1.0 E-05	1.0 E+05	L224F
α_1	1.2 E-02	1.0 E-05	1.0 E+05	L224F
K_{HAMP}	2.4 E+01	1.0 E-05	1.0 E+05	A225F
α_1	2.3 E-01	1.0 E-05	1.0 E+05	A225F
K_{Sen}	1.0 E+03	1.0 E-05	1.0 E+05	A225F
K_{HAMP}	1.1 E+02	1.0 E-05	1.0 E+05	E232A_Gly_7 260/261, E232A
α_2	1.4 E+00	1.0 E-08	1.0 E+02	E232A
K_{HAMP}	2.4 E+01	1.0 E-05	1.0 E+05	E233A
α_2	1.0 E-08	1.0 E-08	1.0 E+02	E233A
K_{HAMP}	8.6 E+00	1.0 E-05	1.0 E+05	R236A
K_{HAMP}	1.7 E+01	1.0 E-05	1.0 E+05	N240A
K_{HAMP}	2.2 E+01	1.0 E-05	1.0 E+05	R245F
K_{AK}	1.0 E-05	1.0 E-05	1.0 E+05	L254A
α_2	1.0 E-08	1.0 E-08	1.0 E+02	L254A
K_{AK}	1.3 E-03	1.0 E-05	1.0 E+05	N255A_Gly_7 260/261, N255A
α_2	4.9 E-01	1.0 E-08	1.0 E+02	N255A
K_{HAMP}	3.6 E+01	1.0 E-05	1.0 E+05	R256A
α_2	1.0 E-08	1.0 E-08	1.0 E+02	R256A
K_{AK}	1.0 E-05	1.0 E-05	1.0 E+05	L258A
α_2	1.0 E-08	1.0 E-08	1.0 E+02	L258A
K_{HAMP}	3.9 E+01	1.0 E-05	1.0 E+05	E261F
α_2	9.9 E-01	1.0 E-08	1.0 E+02	E261F
K_{AK}	4.1 E-04	1.0 E-05	1.0 E+05	Y265A_Gly_7 219/220, Y265A_Gly_7 270/271, Y265A
α_2	3.2 E+00	1.0 E-08	1.0 E+02	Y265A_Gly_7 219/220, Y265A
K_{AK}	3.3 E-03	1.0 E-05	1.0 E+05	R269L
α_2	1.0 E-08	1.0 E-08	1.0 E+02	R269L
K_{HAMP}	4.5 E+01	1.0 E-05	1.0 E+05	Y60C_Gly_7 260/261, Y60C_Gly_4 260/261
α_2	1.0 E+00			Y60C_Gly_7 260;261, Y60C_Gly_4 260/261
α_2	1.0 E+00			S217W_Gly_7 260/261
α_2	1.0 E+00			E232A_Gly_7 260/261
α_2	1.0 E+00			N255A_Gly_7 260/261
α_1	1.0 E+00			Y60C_Gly_7 219/220
α_1	1.0 E+00			S217W_Gly_7 219/220
α_1	1.0 E+00			Y265A_Gly_7 219/220
K_{HAMP}	2.1 E+01	1.0 E-05	1.0 E+05	Y60C_Gly_7 270/271
K_{AK}	7.8 E-04	1.0 E-05	1.0 E+05	Y60C_Gly_7 270/271
α_2	1.7 E+00	1.0 E-08	1.0 E+02	Y60C_Gly_7 270/271
α_2	3.8 E+00	1.0 E-08	1.0 E+02	Y265A_Gly_7 270/271

799

References

1. Stock AM, Robinson VL, Goudreau PN. Two-component signal transduction. Annu Rev Biochem. 2000;69:183–215.

2. Groisman EA, Mouslim C. Sensing by bacterial regulatory systems in host and non-host environments. Nat Rev Microbiol. 2006;4(9):705–9.

3. Nishino K, Honda T, Yamaguchi A. Genome-wide analyses of Escherichia coli gene expression responsive to the BaeSR two-component regulatory system. J Bacteriol. 2005 Mar;187(5):1763–72.

4. Hirakawa H, Nishino K, Hirata T, Yamaguchi A. Comprehensive studies of drug resistance mediated by overexpression of response regulators of two-component signal transduction systems in Escherichia coli. J Bacteriol. 2003 Mar;185(6):1851–6.

5. Nizet V. Antimicrobial peptide resistance mechanisms of human bacterial pathogens. Curr Issues Mol Biol. 2006 Jan;8(1):11–26.

6. Thomas L, Cook L. Two-Component Signal Transduction Systems in the Human Pathogen Streptococcus agalactiae. Infect Immun. 2020 Jun 22;88(7).

7. Delauné A, Dubrac S, Blanchet C, Poupel O, Mäder U, Hiron A, et al. The WalKR system controls major staphylococcal virulence genes and is involved in triggering the host inflammatory response. Infect Immun. 2012 Oct;80(10):3438–53.

8. Ferris HU, Coles M, Lupas AN, Hartmann MD. Crystallographic snapshot of the Escherichia coli EnvZ histidine kinase in an active conformation. J Struct Biol. 2014 Jun;186(3):376–9.

9. Rivera-Cancel G, Ko W, Tomchick DR, Correa F, Gardner KH. Full-length structure of a monomeric histidine kinase reveals basis for sensory regulation. Proc Natl Acad Sci U S A. 2014 Dec 16;111(50):17839–44.

10. Wang C, Sang J, Wang J, Su M, Downey JS, Wu Q, et al. Mechanistic insights revealed by the crystal structure of a histidine kinase with signal transducer and sensor domains. PLoS Biol. 2013;11(2):e1001493.

11. Mechaly AE, Sassoon N, Betton J-M, Alzari PM. Segmental helical motions and dynamical asymmetry modulate histidine kinase autophosphorylation. PLoS Biol. 2014 Jan;12(1):e1001776.

12. Mechaly AE, Soto Diaz S, Sassoon N, Buschiazzo A, Betton J-M, Alzari PM. Structural Coupling between Autokinase and Phosphotransferase Reactions in a Bacterial Histidine Kinase. Struct Lond Engl 1993. 2017 06;25(6):939-944.e3.

13. Casino P, Rubio V, Marina A. Structural insight into partner specificity and phosphoryl transfer in two-component signal transduction. Cell. 2009 Oct 16;139(2):325–36.

14. Albanesi D, Martín M, Trajtenberg F, Mansilla MC, Haouz A, Alzari PM, et al. Structural plasticity and catalysis regulation of a thermosensor histidine kinase. Proc Natl Acad Sci U S A. 2009 Sep 22;106(38):16185–90.

15. Jacob-Dubuisson F, Mechaly A, Betton J-M, Antoine R. Structural insights into the signalling mechanisms of two-component systems. Nat Rev Microbiol. 2018;16(10):585–93.

16. Krell T, Lacal J, Busch A, Silva-Jiménez H, Guazzaroni M-E, Ramos JL. Bacterial sensor kinases: diversity in the recognition of environmental signals. Annu Rev Microbiol. 2010;64:539–59.

17. Bhate MP, Molnar KS, Goulian M, DeGrado WF. Signal transduction in histidine kinases: insights from new structures. Struct Lond Engl 1993. 2015 Jun 2;23(6):981–94.

18. Miller SI, Kukral AM, Mekalanos JJ. A two-component regulatory system (phoP phoQ) controls Salmonella typhimurium virulence. Proc Natl Acad Sci U S A. 1989 Jul;86(13):5054–8.

19. García Véscovi E, Soncini FC, Groisman EA. Mg2+ as an extracellular signal: environmental regulation of Salmonella virulence. Cell. 1996 Jan 12;84(1):165–74.

20. Soncini FC, García Véscovi E, Solomon F, Groisman EA. Molecular basis of the magnesium deprivation response in Salmonella typhimurium: identification of PhoP-regulated genes. J Bacteriol. 1996 Sep;178(17):5092–9.

21. Bader MW, Sanowar S, Daley ME, Schneider AR, Cho U, Xu W, et al. Recognition of antimicrobial peptides by a bacterial sensor kinase. Cell. 2005 Aug 12;122(3):461–72.

22. Hancock REW, McPhee JB. Salmonella's sensor for host defense molecules. Cell. 2005 Aug 12;122(3):320–2.

23. Groisman EA, Chiao E, Lipps CJ, Heffron F. Salmonella typhimurium phoP virulence gene is a transcriptional regulator. Proc Natl Acad Sci U S A. 1989 Sep;86(18):7077–81.

24. Fields PI, Groisman EA, Heffron F. A Salmonella locus that controls resistance to microbicidal proteins from phagocytic cells. Science. 1989 Feb 24;243(4894 Pt 1):1059–62.

25. Behlau I, Miller SI. A PhoP-repressed gene promotes Salmonella typhimurium invasion of epithelial cells. J Bacteriol. 1993 Jul;175(14):4475–84.

26. Belden WJ, Miller SI. Further characterization of the PhoP regulon: identification of new PhoP-activated virulence loci. Infect Immun. 1994 Nov;62(11):5095–101.

27. Gunn JS, Miller SI. PhoP-PhoQ activates transcription of pmrAB, encoding a two-component regulatory system involved in Salmonella typhimurium antimicrobial peptide resistance. J Bacteriol. 1996 Dec;178(23):6857–64.

28. Guo L, Lim KB, Gunn JS, Bainbridge B, Darveau RP, Hackett M, et al. Regulation of lipid A modifications by Salmonella typhimurium virulence genes phoP-phoQ. Science. 1997 Apr 11;276(5310):250–3.

29. Bearson BL, Wilson L, Foster JW. A low pH-inducible, PhoPQ-dependent acid tolerance response protects Salmonella typhimurium against inorganic acid stress. J Bacteriol. 1998 May;180(9):2409–17.

30. Guo L, Lim KB, Poduje CM, Daniel M, Gunn JS, Hackett M, et al. Lipid A acylation and bacterial resistance against vertebrate antimicrobial peptides. Cell. 1998 Oct 16;95(2):189–98.

31. Adams P, Fowler R, Kinsella N, Howell G, Farris M, Coote P, et al. Proteomic detection of PhoPQ- and acid-mediated repression of Salmonella motility. Proteomics. 2001 Apr;1(4):597–607.

32. Bader MW, Navarre WW, Shiau W, Nikaido H, Frye JG, McClelland M, et al. Regulation of Salmonella typhimurium virulence gene expression by cationic antimicrobial peptides. Mol Microbiol. 2003 Oct;50(1):219–30.

33. Dalebroux ZD, Matamouros S, Whittington D, Bishop RE, Miller SI. PhoPQ regulates acidic glycerophospholipid content of the Salmonella Typhimurium outer membrane. Proc Natl Acad Sci U S A. 2014 Feb 4;111(5):1963–8.

34. Prost LR, Daley ME, Le Sage V, Bader MW, Le Moual H, Klevit RE, et al. Activation of the bacterial sensor kinase PhoQ by acidic pH. Mol Cell. 2007 Apr 27;26(2):165–74.

35. Choi J, Groisman EA. Activation of master virulence regulator PhoP in acidic pH requires the Salmonella-specific protein UgtL. Sci Signal. 2017 Aug 29;10(494).

36. Yuan J, Jin F, Glatter T, Sourjik V. Osmosensing by the bacterial PhoQ/PhoP two-component system. Proc Natl Acad Sci U S A. 2017 12;114(50):E10792–8.

37. Cho US, Bader MW, Amaya MF, Daley ME, Klevit RE, Miller SI, et al. Metal bridges between the PhoQ sensor domain and the membrane regulate transmembrane signaling. J Mol Biol. 2006 Mar 10;356(5):1193–206.

38. Chamnongpol S, Cromie M, Groisman EA. Mg2+ sensing by the Mg2+ sensor PhoQ of Salmonella enterica. J Mol Biol. 2003 Jan 24;325(4):795–807.

39. Miyashiro T, Goulian M. Stimulus-dependent differential regulation in the Escherichia coli PhoQ PhoP system. Proc Natl Acad Sci U S A. 2007 Oct 9;104(41):16305–10.

40. Falke JJ, Hazelbauer GL. Transmembrane signaling in bacterial chemoreceptors. Trends Biochem Sci. 2001 Apr;26(4):257–65.

902 41. Draheim RR, Bormans AF, Lai R, Manson MD. Tryptophan residues flanking the second
903 transmembrane helix (TM2) set the signaling state of the Tar chemoreceptor. Biochemistry.
904 2005 Feb 1;44(4):1268–77.

905 42. Bornhorst JA, Falke JJ. Attractant regulation of the aspartate receptor-kinase complex:
906 limited cooperative interactions between receptors and effects of the receptor modification
907 state. Biochemistry. 2000 Aug 8;39(31):9486–93.

908 43. Waldburger CD, Sauer RT. Signal detection by the PhoQ sensor-transmitter.
909 Characterization of the sensor domain and a response-impaired mutant that identifies
910 ligand-binding determinants. J Biol Chem. 1996 Oct 25;271(43):26630–6.

911 44. Keller R, Ariöz C, Hansmeier N, Stenberg-Bruzell F, Burstedt M, Vikström D, et al. The
912 Escherichia coli Envelope Stress Sensor CpxA Responds to Changes in Lipid Bilayer
913 Properties. Biochemistry. 2015 Jun 16;54(23):3670–6.

914 45. Batchelor E, Walthers D, Kenney LJ, Goulian M. The Escherichia coli CpxA-CpxR
915 envelope stress response system regulates expression of the porins ompF and ompC. J
916 Bacteriol. 2005 Aug;187(16):5723–31.

917 46. Danese PN, Silhavy TJ. The sigma(E) and the Cpx signal transduction systems control the
918 synthesis of periplasmic protein-folding enzymes in Escherichia coli. Genes Dev. 1997
919 May 1;11(9):1183–93.

920 47. Zhou X, Keller R, Volkmer R, Krauss N, Scheerer P, Hunke S. Structural basis for two-
921 component system inhibition and pilus sensing by the auxiliary CpxP protein. J Biol Chem.
922 2011 Mar 18;286(11):9805–14.

923 48. Leblanc SKD, Oates CW, Raivio TL. Characterization of the induction and cellular role of
924 the BaeSR two-component envelope stress response of Escherichia coli. J Bacteriol. 2011
925 Jul;193(13):3367–75.

926 49. Clark IC, Mensa B, Ochs CJ, Schmidt NW, Mravic M, Quintana FJ, et al. Protein design-
927 scapes generated by microfluidic DNA assembly elucidate domain coupling in the bacterial
928 histidine kinase CpxA. Proc Natl Acad Sci U S A. 2021 Mar 23;118(12):e2017719118.

929 50. Mensa B, Kim YH, Choi S, Scott R, Caputo GA, DeGrado WF. Antibacterial mechanism of
930 action of arylamide foldamers. Antimicrob Agents Chemother. 2011 Nov;55(11):5043–53.

931 51. Fernández P, Porrini L, Albanesi D, Abriata LA, Dal Peraro M, de Mendoza D, et al.
932 Transmembrane Prolines Mediate Signal Sensing and Decoding in Bacillus subtilis DesK
933 Histidine Kinase. mBio. 2019 26;10(6).

934 52. Wang LC, Morgan LK, Godakumbura P, Kenney LJ, Anand GS. The inner membrane
935 histidine kinase EnvZ senses osmolality via helix-coil transitions in the cytoplasm. EMBO
936 J. 2015 Oct 1;34(19):2481.

53. Koh A, Gibbon MJ, Van der Kamp MW, Pudney CR, Gebhard S. Conformation control of the histidine kinase BceS of Bacillus subtilis by its cognate ABC-transporter facilitates need-based activation of antibiotic resistance. Mol Microbiol. 2021 Jan;115(1):157–74.

54. Matamouros S, Hager KR, Miller SI. HAMP Domain Rotation and Tilting Movements Associated with Signal Transduction in the PhoQ Sensor Kinase. mBio. 2015 May 26;6(3):e00616-00615.

55. Baruah A, Lindsey B, Zhu Y, Nakano MM. Mutational analysis of the signal-sensing domain of ResE histidine kinase from Bacillus subtilis. J Bacteriol. 2004 Mar;186(6):1694–704.

56. Eguchi Y, Utsumi R. Alkali metals in addition to acidic pH activate the EvgS histidine kinase sensor in Escherichia coli. J Bacteriol. 2014 Sep;196(17):3140–9.

57. Gao R, Lynn DG. Environmental pH sensing: resolving the VirA/VirG two-component system inputs for Agrobacterium pathogenesis. J Bacteriol. 2005 Mar;187(6):2182–9.

58. Edelstein SJ, Changeux JP. Allosteric proteins after thirty years: the binding and state functions of the neuronal alpha 7 nicotinic acetylcholine receptors. Experientia. 1996 Dec 15;52(12):1083–90.

59. Ashenberg O, Rozen-Gagnon K, Laub MT, Keating AE. Determinants of homodimerization specificity in histidine kinases. J Mol Biol. 2011 Oct 14;413(1):222–35.

60. Podgornaia AI, Casino P, Marina A, Laub MT. Structural basis of a rationally rewired protein-protein interface critical to bacterial signaling. Struct Lond Engl 1993. 2013 Sep 3;21(9):1636–47.

61. Skerker JM, Perchuk BS, Siryaporn A, Lubin EA, Ashenberg O, Goulian M, et al. Rewiring the specificity of two-component signal transduction systems. Cell. 2008 Jun 13;133(6):1043–54.

62. Buschiazzo A, Trajtenberg F. Two-Component Sensing and Regulation: How Do Histidine Kinases Talk with Response Regulators at the Molecular Level? Annu Rev Microbiol. 2019 08;73:507–28.

63. Ohta N, Newton A. The core dimerization domains of histidine kinases contain recognition specificity for the cognate response regulator. J Bacteriol. 2003 Aug;185(15):4424–31.

64. Salazar ME, Laub MT. Temporal and evolutionary dynamics of two-component signaling pathways. Curr Opin Microbiol. 2015 Apr;24:7–14.

65. Anantharaman V, Balaji S, Aravind L. The signaling helix: a common functional theme in diverse signaling proteins. Biol Direct. 2006 Sep 5;1:25.

970 66. Schmidt NW, Grigoryan G, DeGrado WF. The accommodation index measures the
971 perturbation associated with insertions and deletions in coiled-coils: Application to
972 understand signaling in histidine kinases. Protein Sci Publ Protein Soc. 2017;26(3):414–35.

973 67. Motz M, Jung K. The role of polyproline motifs in the histidine kinase EnvZ. PloS One.
974 2018;13(6):e0199782.

975 68. Akkaladevi N, Bunyak F, Stalla D, White TA, Hazelbauer GL. Flexible Hinges in Bacterial
976 Chemoreceptors. J Bacteriol. 2018 01;200(5).

977 69. Inouye M. Signaling by transmembrane proteins shifts gears. Cell. 2006 Sep 8;126(5):829–
978 31.

979 70. Chervitz SA, Falke JJ. Molecular mechanism of transmembrane signaling by the aspartate
980 receptor: a model. Proc Natl Acad Sci U S A. 1996 Mar 19;93(6):2545–50.

981 71. Falke JJ, Erbse AH. The piston rises again. Struct Lond Engl 1993. 2009 Sep 9;17(9):1149–
982 51.

983 72. Molnar KS, Bonomi M, Pellarin R, Clinthorne GD, Gonzalez G, Goldberg SD, et al. Cys-
984 scanning disulfide crosslinking and bayesian modeling probe the transmembrane signaling
985 mechanism of the histidine kinase, PhoQ. Struct Lond Engl 1993. 2014 Sep 2;22(9):1239–
986 51.

987 73. Milburn MV, Privé GG, Milligan DL, Scott WG, Yeh J, Jancarik J, et al. Three-
988 dimensional structures of the ligand-binding domain of the bacterial aspartate receptor with
989 and without a ligand. Science. 1991 Nov 29;254(5036):1342–7.

990 74. Lowe EC, Baslé A, Czjzek M, Firbank SJ, Bolam DN. A scissor blade-like closing
991 mechanism implicated in transmembrane signaling in a Bacteroides hybrid two-component
992 system. Proc Natl Acad Sci U S A. 2012 May 8;109(19):7298–303.

993 75. Airola MV, Watts KJ, Bilwes AM, Crane BR. Structure of concatenated HAMP domains
994 provides a mechanism for signal transduction. Struct Lond Engl 1993. 2010 Mar
995 14;18(4):436–48.

996 76. Swain KE, Falke JJ. Structure of the conserved HAMP domain in an intact, membrane-
997 bound chemoreceptor: a disulfide mapping study. Biochemistry. 2007 Dec 4;46(48):13684–
998 95.

999 77. Swain KE, Gonzalez MA, Falke JJ. Engineered socket study of signaling through a four-
1000 helix bundle: evidence for a yin-yang mechanism in the kinase control module of the
1001 aspartate receptor. Biochemistry. 2009 Oct 6;48(39):9266–77.

1002 78. Parkinson JS. Signaling mechanisms of HAMP domains in chemoreceptors and sensor
1003 kinases. Annu Rev Microbiol. 2010;64:101–22.

79. Stewart V. The HAMP signal-conversion domain: static two-state or dynamic three-state? Mol Microbiol. 2014 Mar;91(5):853–7.

80. Ferris HU, Dunin-Horkawicz S, Mondéjar LG, Hulko M, Hantke K, Martin J, et al. The mechanisms of HAMP-mediated signaling in transmembrane receptors. Struct Lond Engl 1993. 2011 Mar 9;19(3):378–85.

81. Gushchin I, Melnikov I, Polovinkin V, Ishchenko A, Yuzhakova A, Buslaev P, et al. Mechanism of transmembrane signaling by sensor histidine kinases. Science. 2017 09;356(6342).

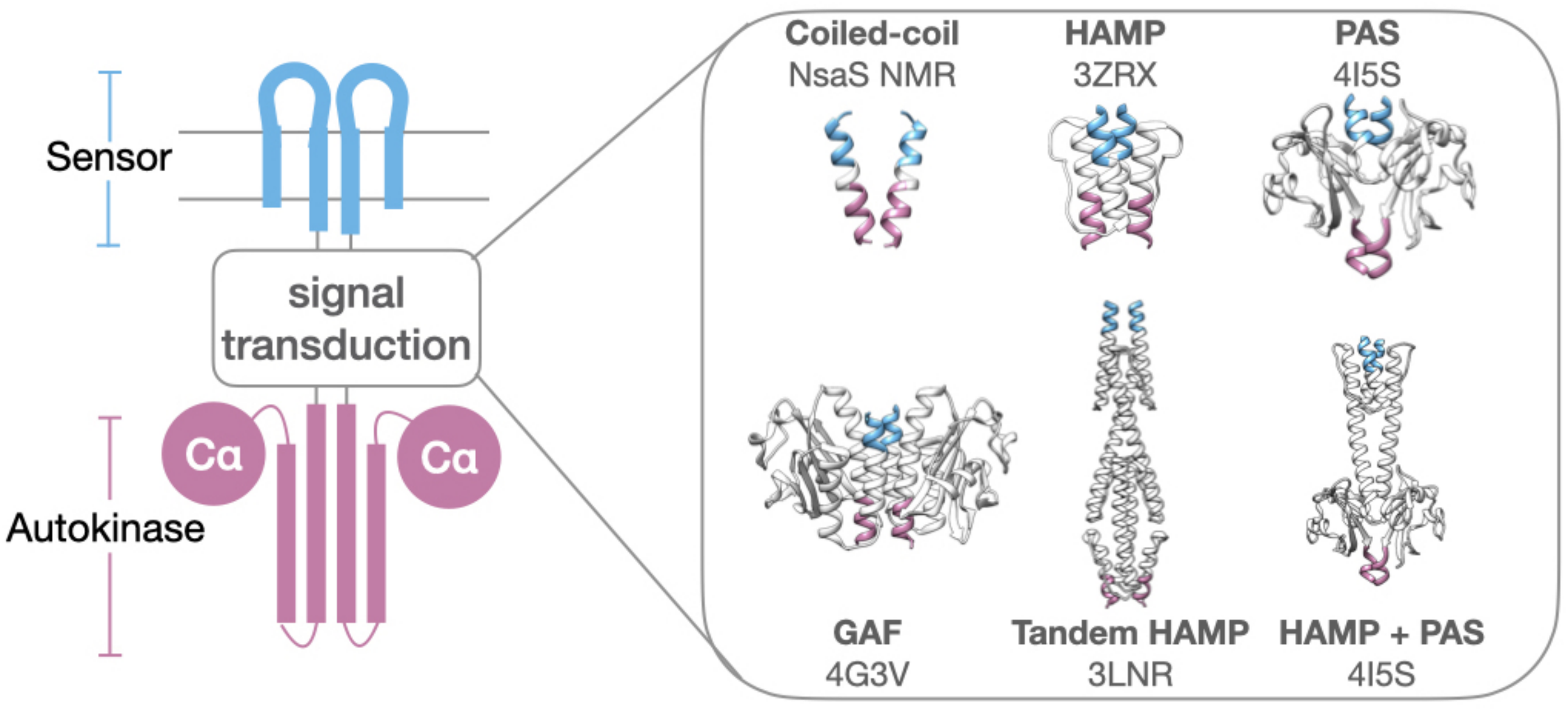
Sensor
signal transduction
Cα
Cα
Autokinase
Coiled-coil
NsaS NMR
HAMP
3ZRX
PAS
4I5S
GAF
4G3V
Tandem HAMP
3LNR
HAMP + PAS
4I5S

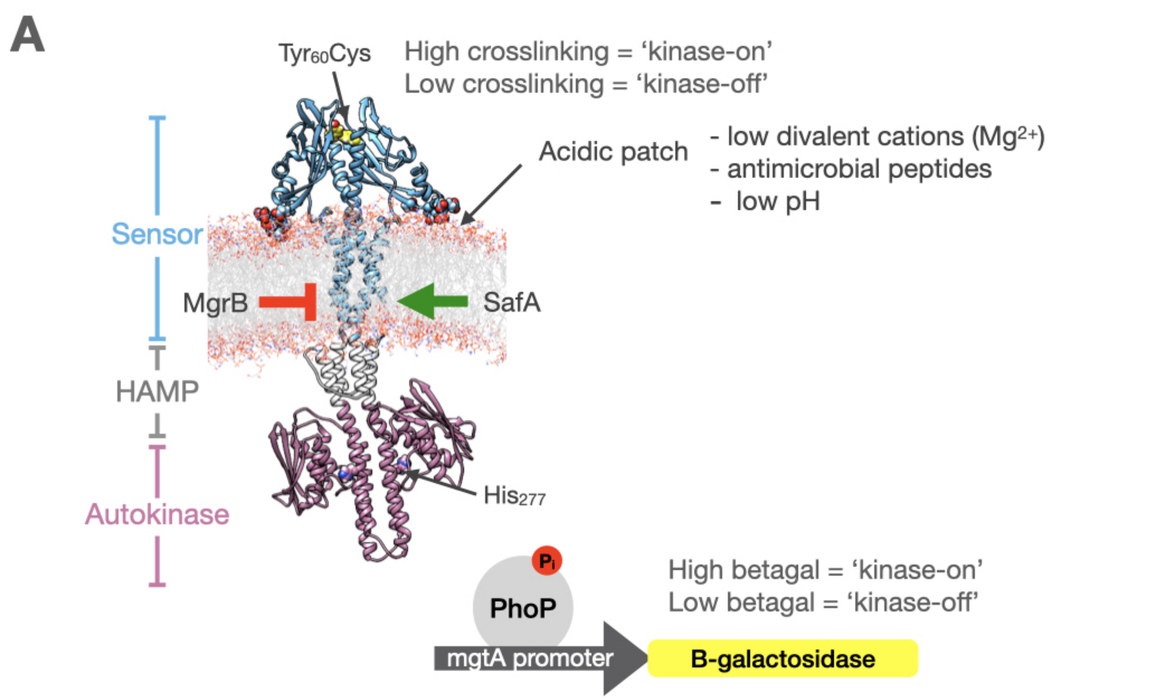

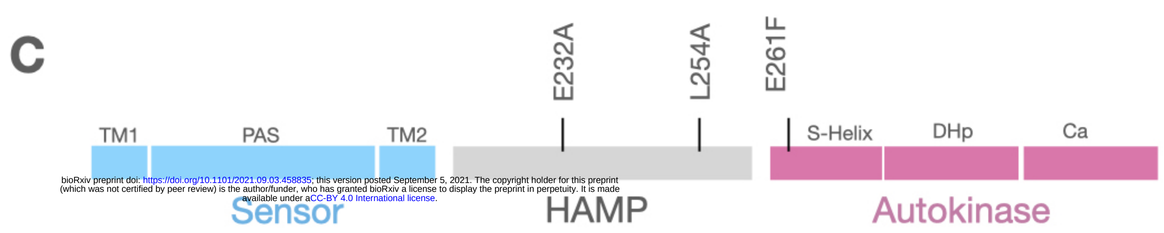

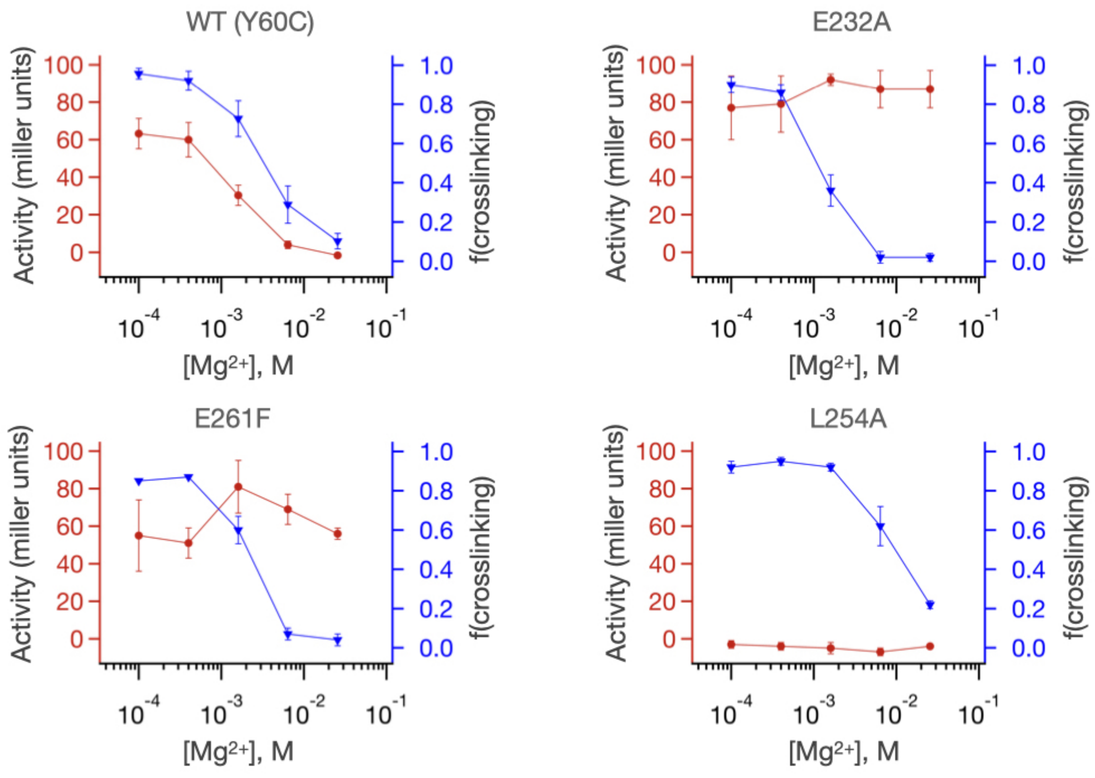

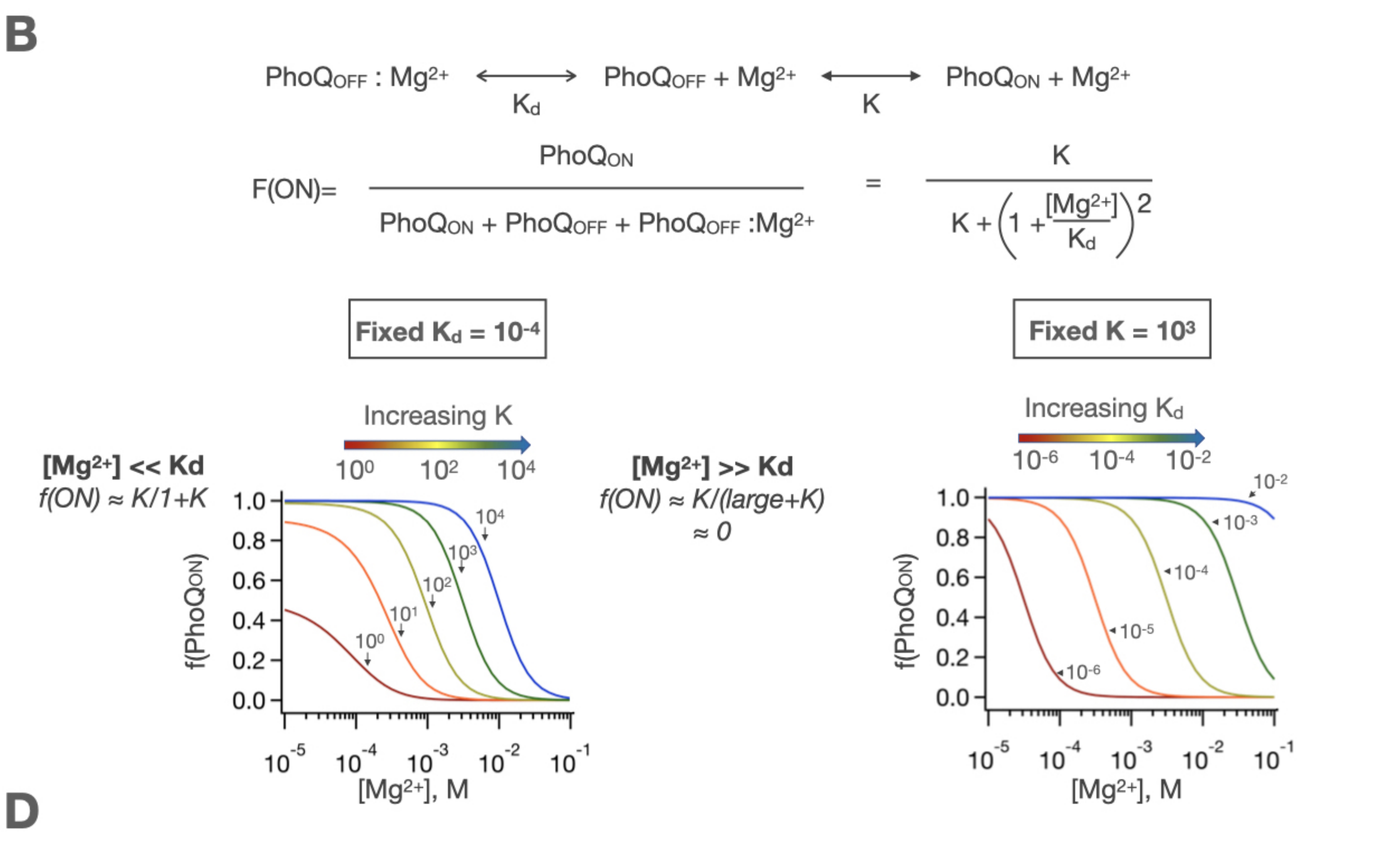

A

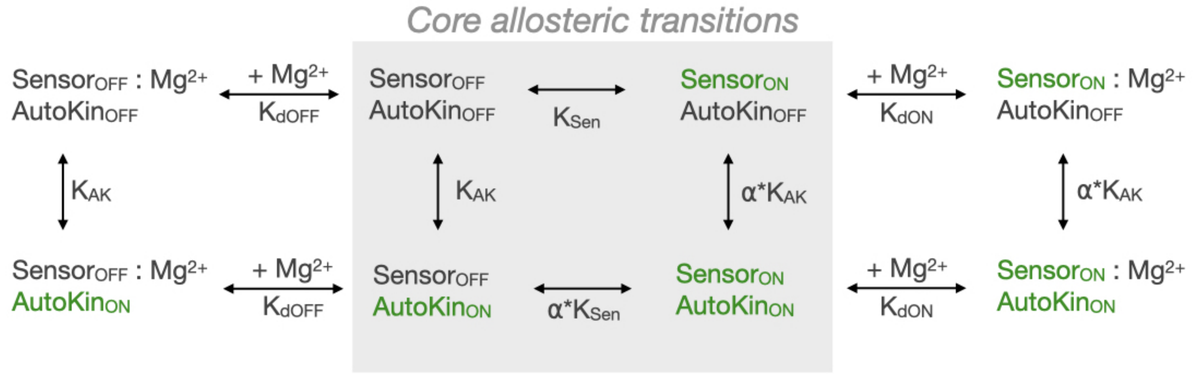

$$F(Sensor_{ON}) = \frac{Sen_{ON}AK_{OFF} + Sen_{ON}AK_{ON}}{All} = \frac{\left(1+\frac{[Mg^{2+}]}{K_{dON}}\right)^2 * (K_{Sen} + \alpha K_{Sen}K_{AK})}{\left(1+\frac{[Mg^{2+}]}{K_{dON}}\right)^2 * (K_{Sen} + \alpha K_{Sen}K_{AK}) + \left(1+\frac{[Mg^{2+}]}{K_{dOFF}}\right)^2 * (1 + K_{AK})}$$

$$F(AutoKin_{ON}) = \frac{Sen_{ON}AK_{ON} + Sen_{OFF}AK_{ON}}{All} = \frac{\left(1+\frac{[Mg^{2+}]}{K_{dON}}\right)^2 * \alpha K_{Sen}K_{AK} + \left(1+\frac{[Mg^{2+}]}{K_{dOFF}}\right)^2 * K_{AK}}{\left(1+\frac{[Mg^{2+}]}{K_{dON}}\right)^2 * (K_{Sen} + \alpha K_{Sen}K_{AK}) + \left(1+\frac{[Mg^{2+}]}{K_{dOFF}}\right)^2 * (1 + K_{AK})}$$

B

Sensor and autokinase uncoupled
(α=1)

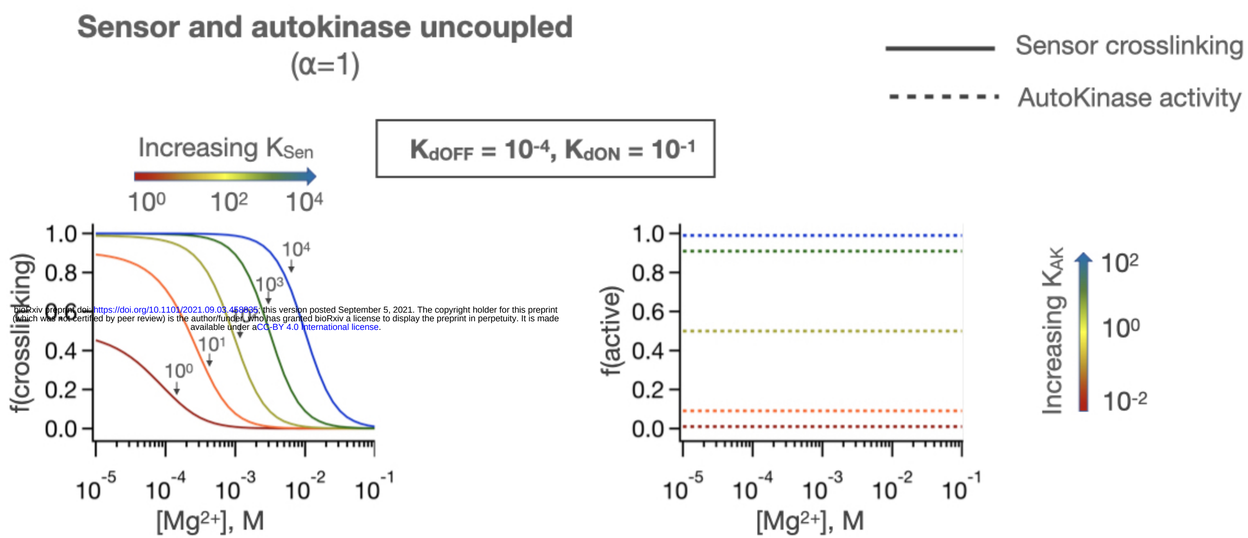

C

Sensor and autokinase coupled
Effect of coupling strength (α)

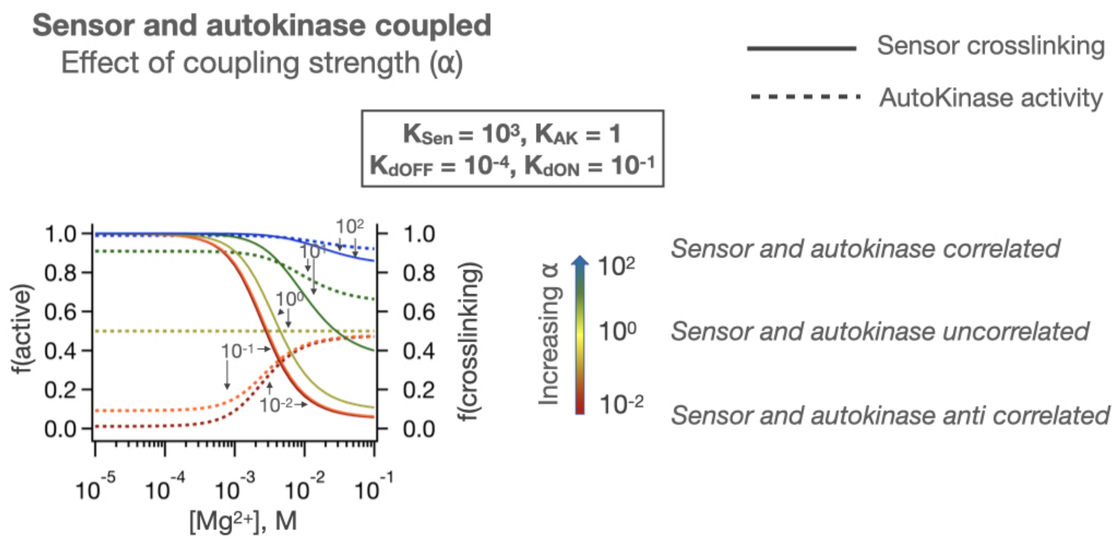

D

Effect of K$_{Sen}$

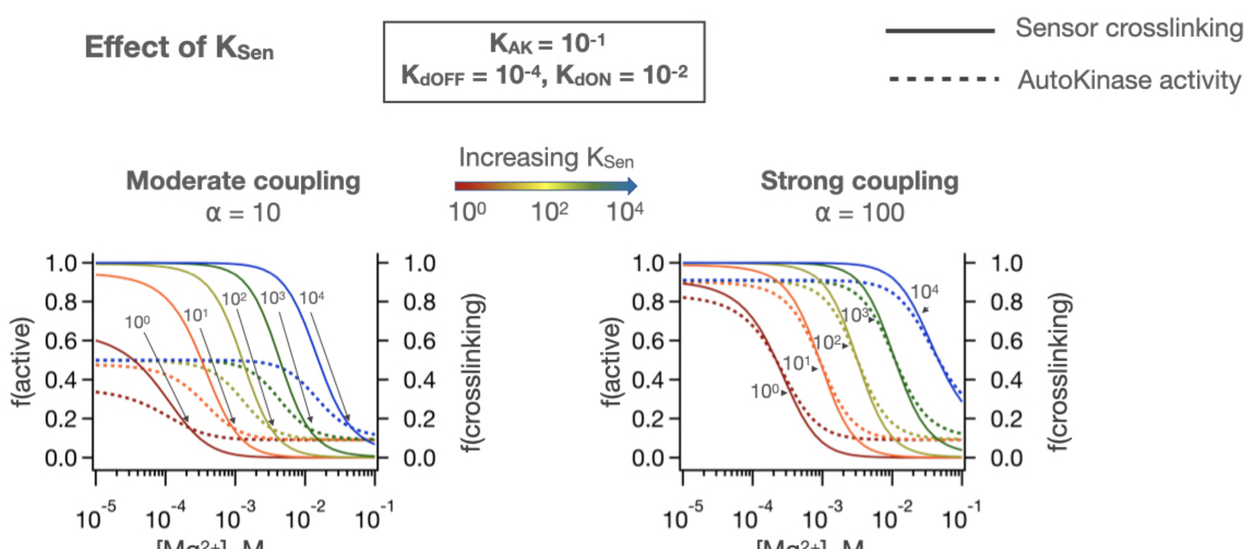

E

Effect of K$_{AK}$

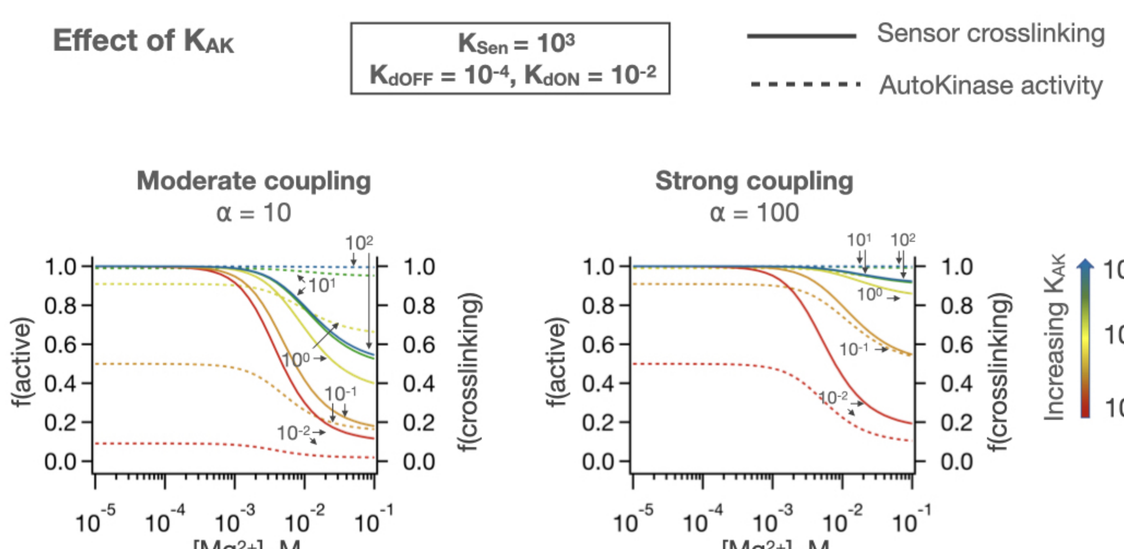

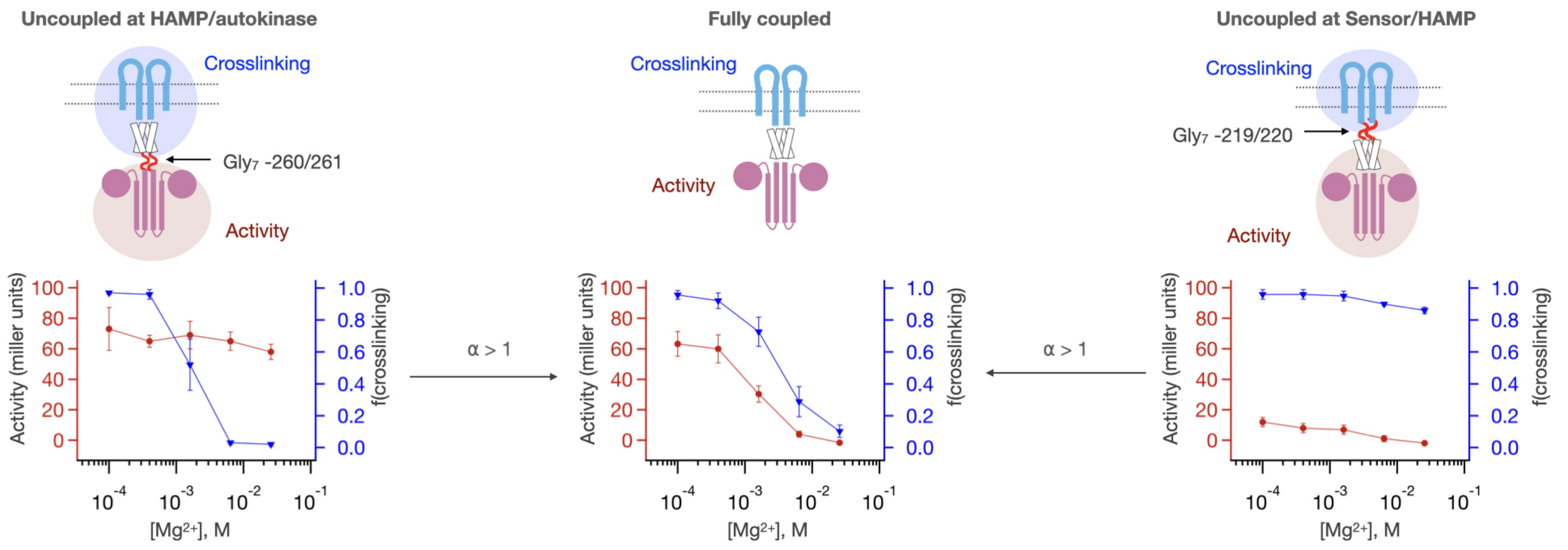
Uncoupled at HAMP/autokinase
Crosslinking
Gly7 -260/261
Activity
Fully coupled
Crosslinking
Activity
Uncoupled at Sensor/HAMP
Crosslinking
Gly7 -219/220
Activity
α > 1
α > 1
Activity (miller units)
f(crosslinking)
[Mg2+], M
100
80
60
40
20
0
1.0
0.8
0.6
0.4
0.2
0.0
10-4
10-3
10-2
10-1

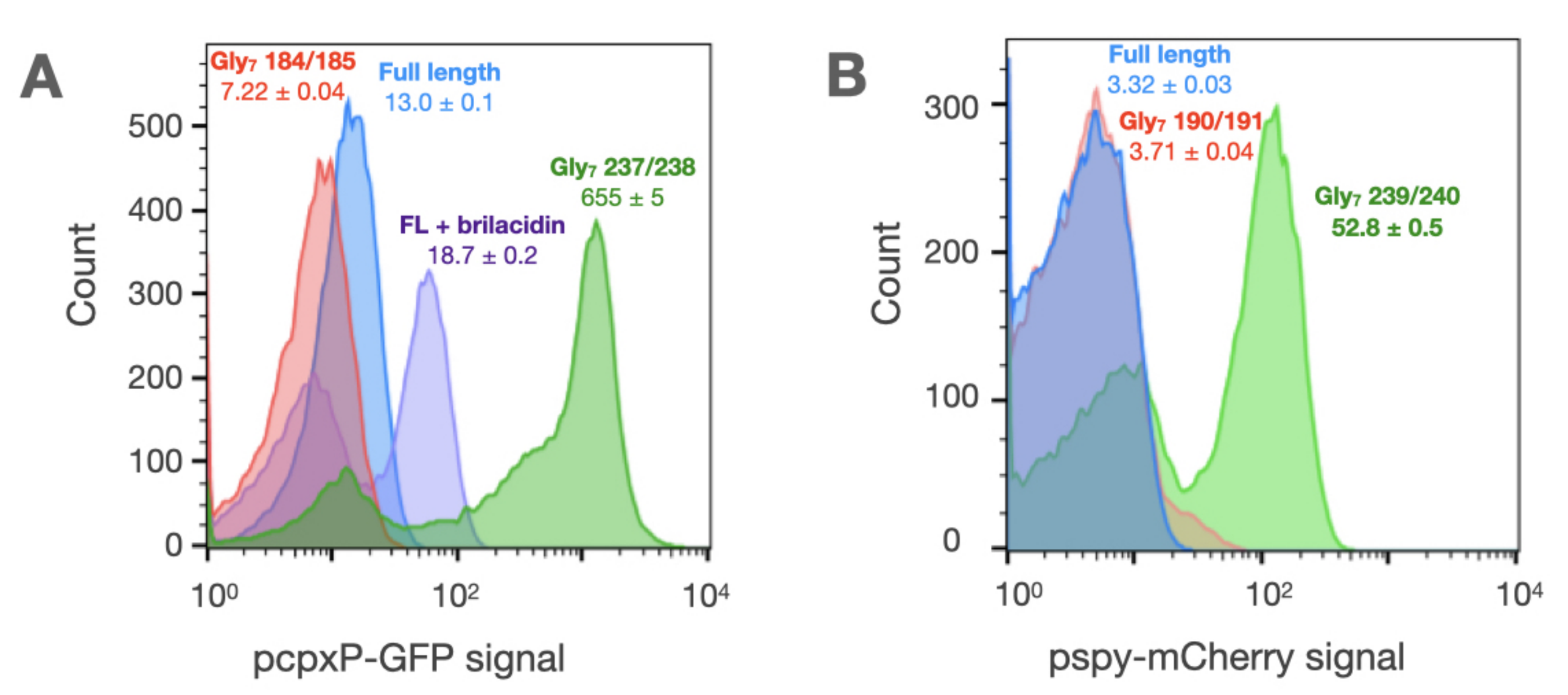
A
Gly7 184/185
7.22 ± 0.04
Full length
13.0 ± 0.1
Gly7 237/238
655 ± 5
FL + brilacidin
18.7 ± 0.2
Count
500
400
300
200
100
0
10^0
10^2
10^4
pcpxP-GFP signal
B
Full length
3.32 ± 0.03
Gly7 190/191
3.71 ± 0.04
Gly7 239/240
52.8 ± 0.5
Count
300
200
100
0
10^0
10^2
10^4
pspy-mCherry signal

A

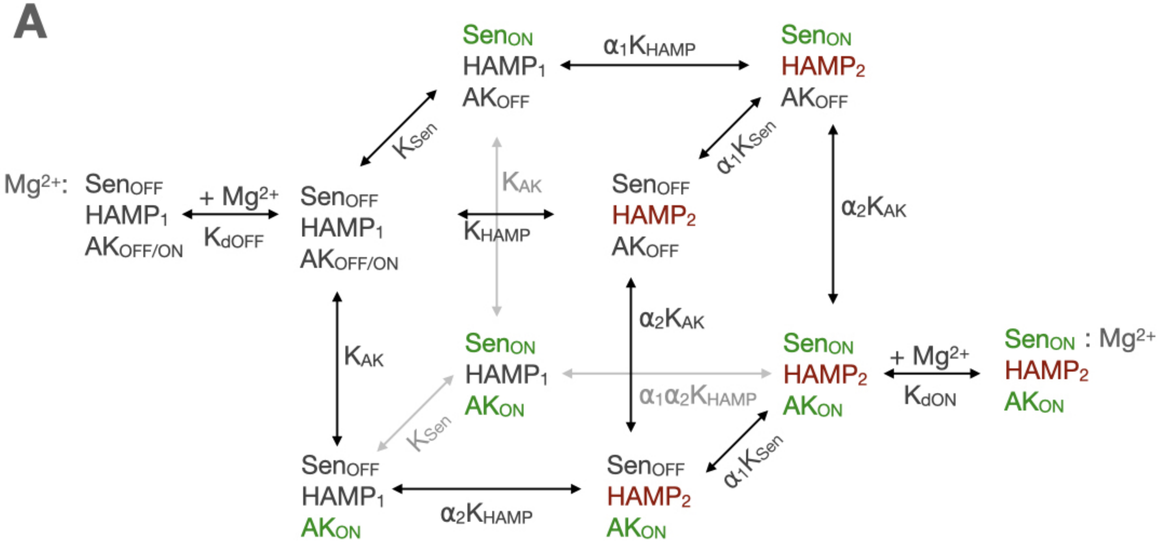

$$F(Sensor_{ON}) = \frac{Sen_{ON}HAMP_1AK_{OFF} + Sen_{ON}HAMP_1AK_{ON} + Sen_{ON}HAMP_2AK_{OFF} + Sen_{ON}HAMP_2AK_{ON}}{All}$$

$$= \frac{\left(1+\frac{[Mg^{2+}]}{K_{dON}}\right)^2 * (K_{sen} + K_{Sen}K_{AK} + \alpha_1 K_{Sen}K_{HAMP} + \alpha_1\alpha_2 K_{Sen}K_{HAMP}K_{AK})}{\left(1+\frac{[Mg^{2+}]}{K_{dON}}\right)^2 * (K_{Sen} + K_{sen}K_{AK} + \alpha_1 K_{Sen}K_{HAMP} + \alpha_1\alpha_2 K_{Sen}K_{HAMP}K_{AK}) + \left(1+\frac{[Mg^{2+}]}{K_{dOFF}}\right)^2 * (1 + K_{AK} + K_{HAMP} + \alpha_2 K_{HAMP}K_{AK})}$$

$$F(AutoKin_{ON}) = \frac{Sen_{OFF}HAMP_1AK_{ON} + Sen_{OFF}HAMP_2AK_{ON} + Sen_{ON}HAMP_1AK_{ON} + Sen_{ON}HAMP_2AK_{ON}}{All}$$

$$= \frac{\left(1+\frac{[Mg^{2+}]}{K_{dOFF}}\right)^2 * (K_{AK} + \alpha_2 K_{HAMP}K_{AK}) + \left(1+\frac{[Mg^{2+}]}{K_{dON}}\right)^2 * (K_{sen}K_{AK} + \alpha_1\alpha_2 K_{Sen}K_{HAMP}K_{AK})}{\left(1+\frac{[Mg^{2+}]}{K_{dON}}\right)^2 * (K_{Sen} + K_{sen}K_{AK} + \alpha_1 K_{Sen}K_{HAMP} + \alpha_1\alpha_2 K_{Sen}K_{HAMP}K_{AK}) + \left(1+\frac{[Mg^{2+}]}{K_{dOFF}}\right)^2 * (1 + K_{AK} + K_{HAMP} + \alpha_2 K_{HAMP}K_{AK})}$$

B

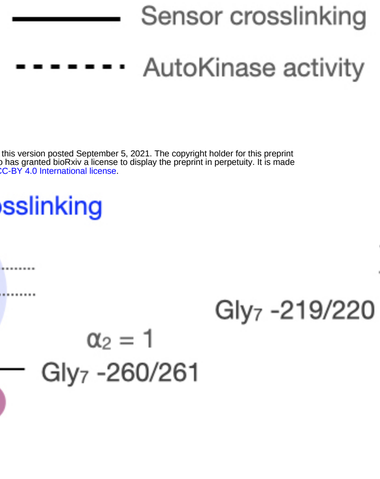

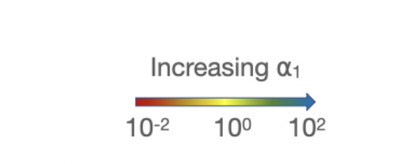

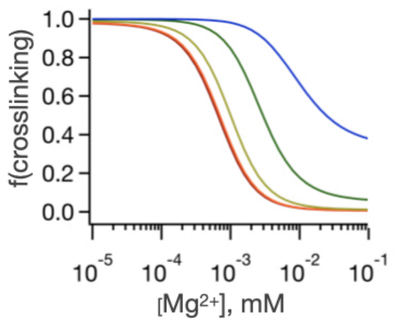

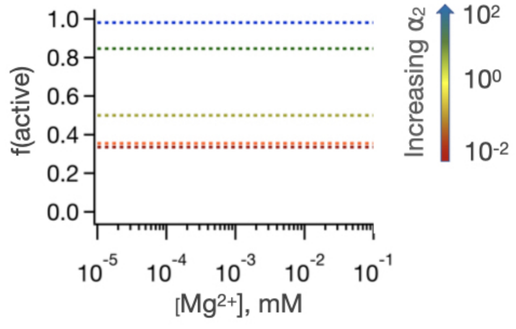

C

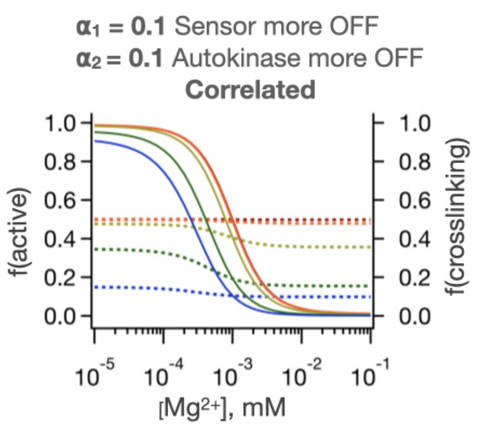

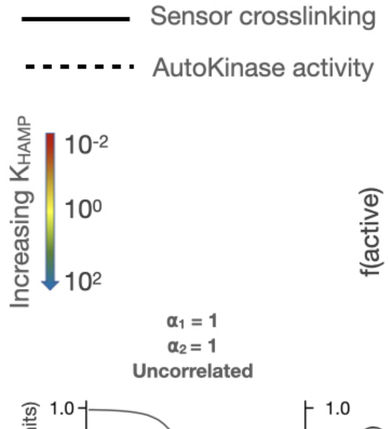

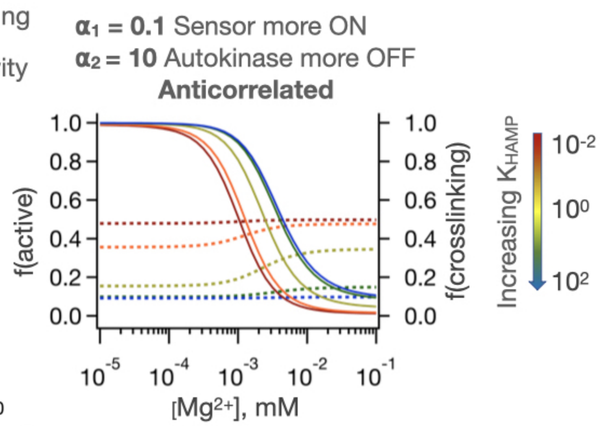

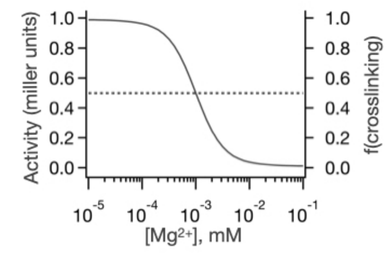

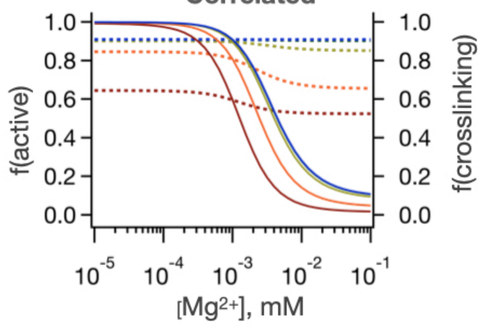

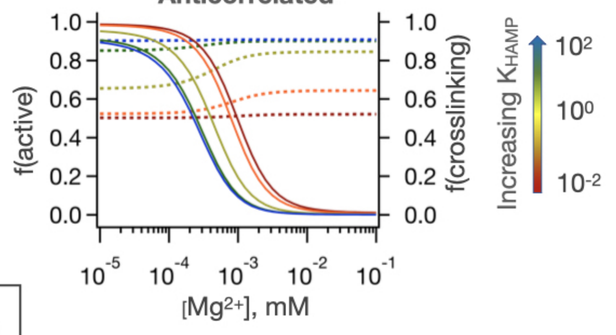

$K_{Sen} = 10^3$, $K_{AK} = 1$
$K_{dOFF} = 10^{-4}$, $K_{dON} = 10^{-2}$

A

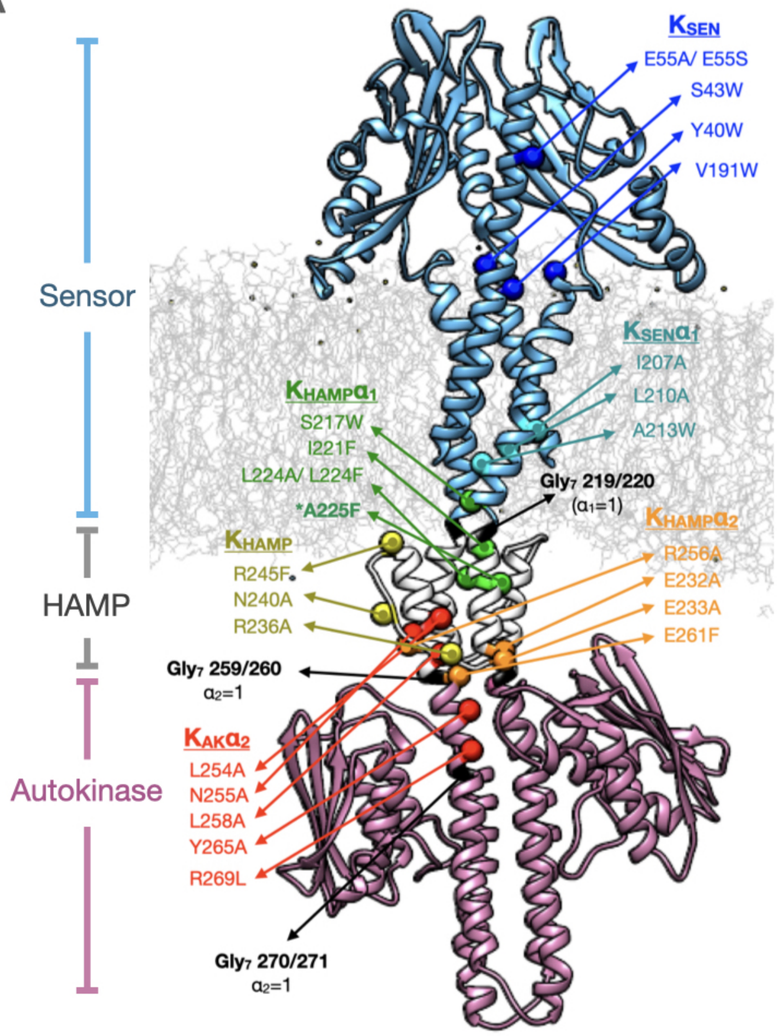

B

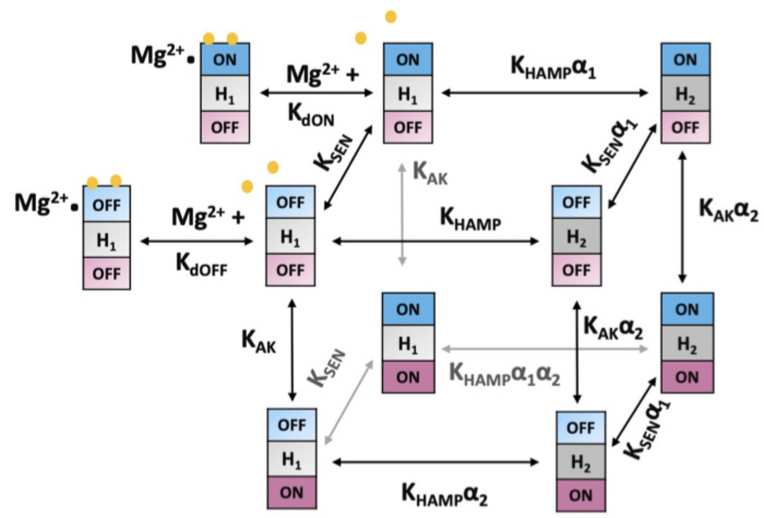

$$F(Sensor_{ON}) = \frac{ONH_1OFF + ONH_1ON + ONH_2OFF + ONH_2ON}{All}$$

$$F(AutoKin_{ON}) = \frac{ONH_1ON + OFFH_1ON + OFFH_2ON + ONH_2ON}{All}$$

C

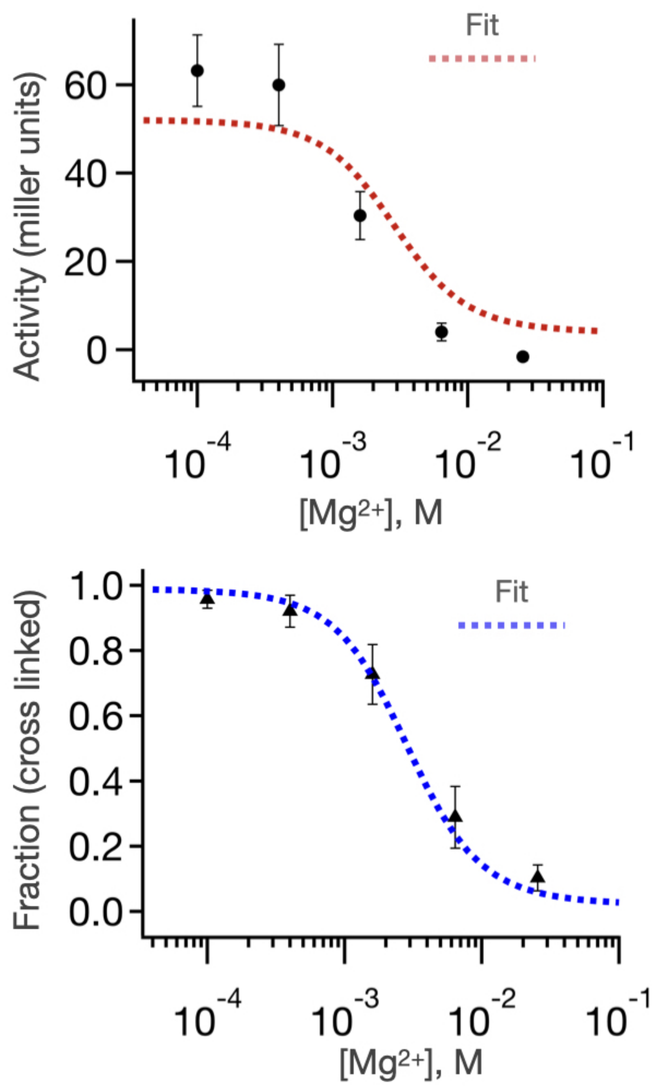

D

K_{dON} = 1.62 x10^{-2} | K_{dOFF} = 3.66 x 10^{-4} | α_1 = 5.30 x 10^{-3} | α_2 = 10^{-8}

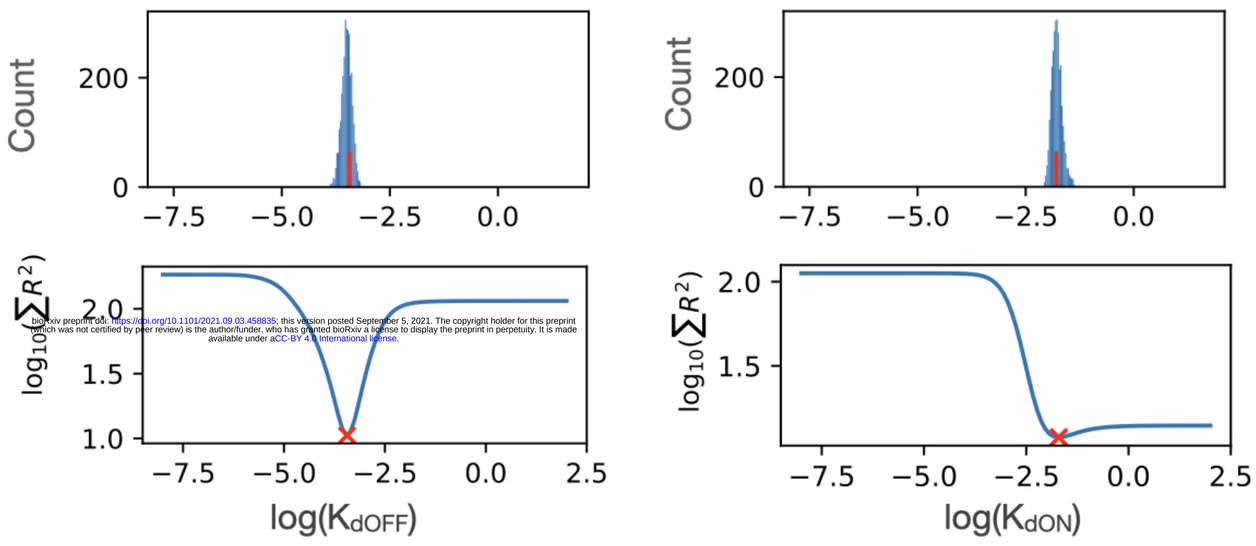

K_{SEN} = 9.51 x10^{2} | K_{HAMP} = 2.22 x 10^{1} | K_{AK} = 1.38 x 10^{-3} | S = 7.43x 10^{2}

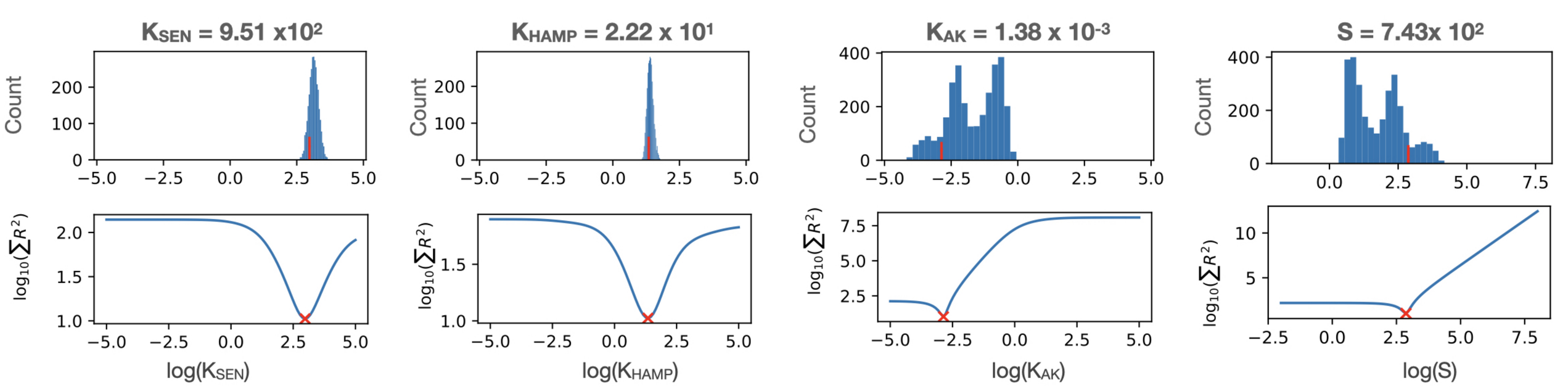

Range of S

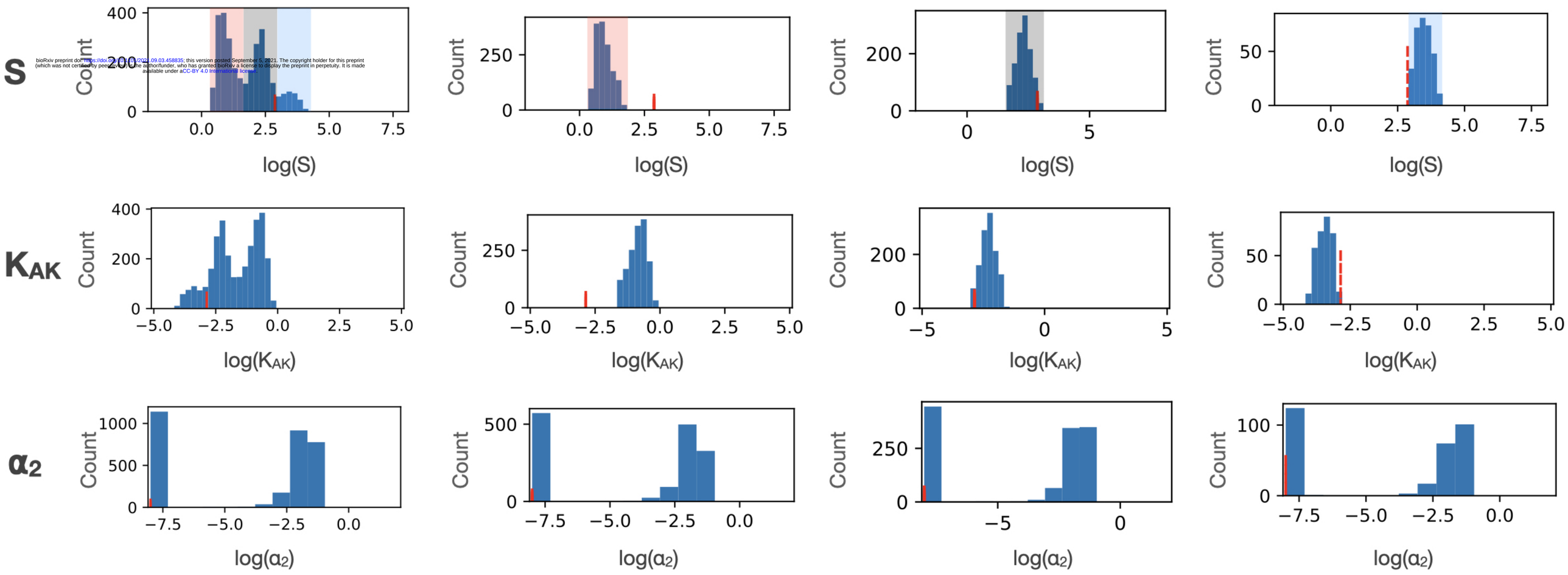

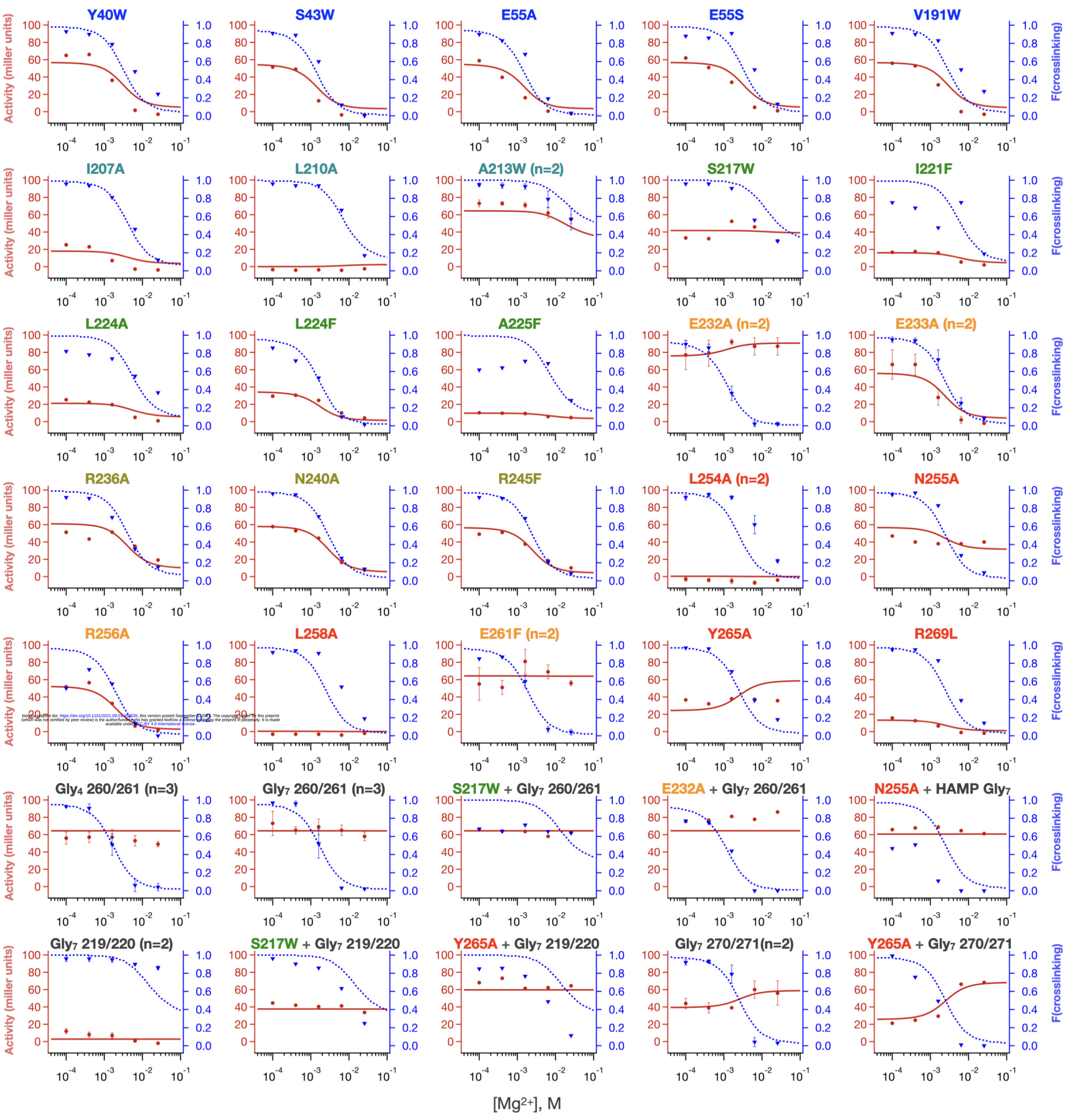

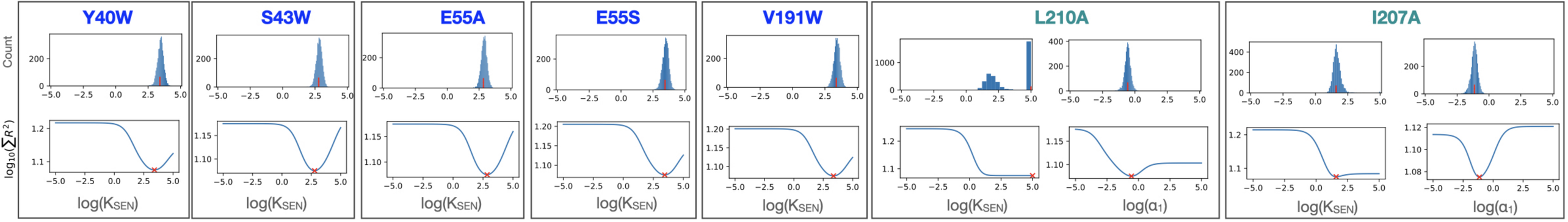

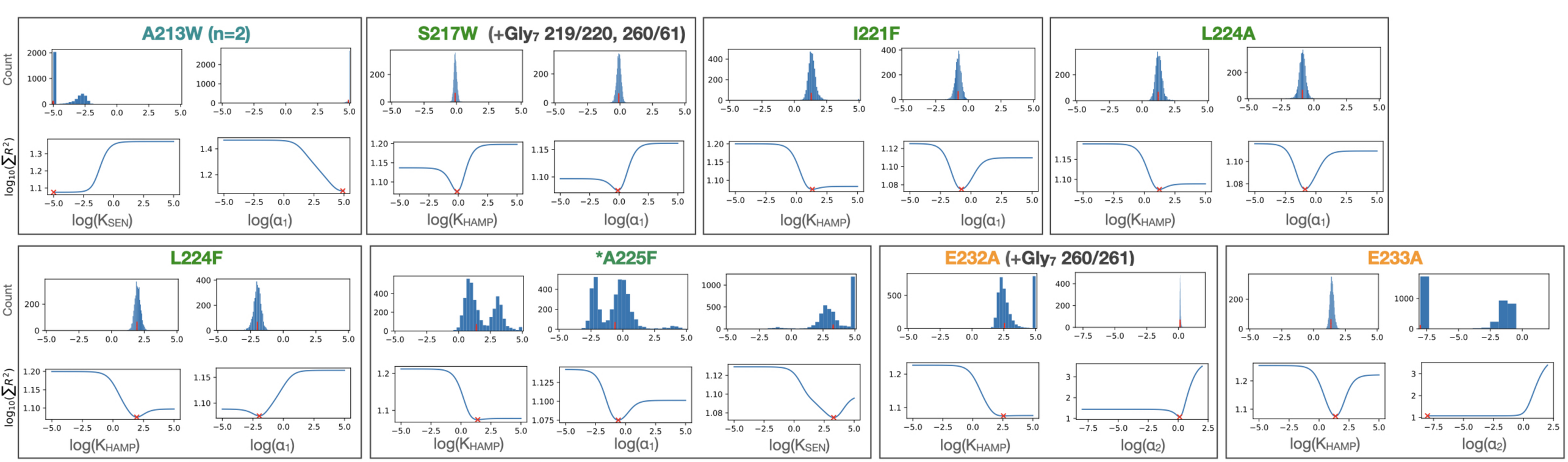

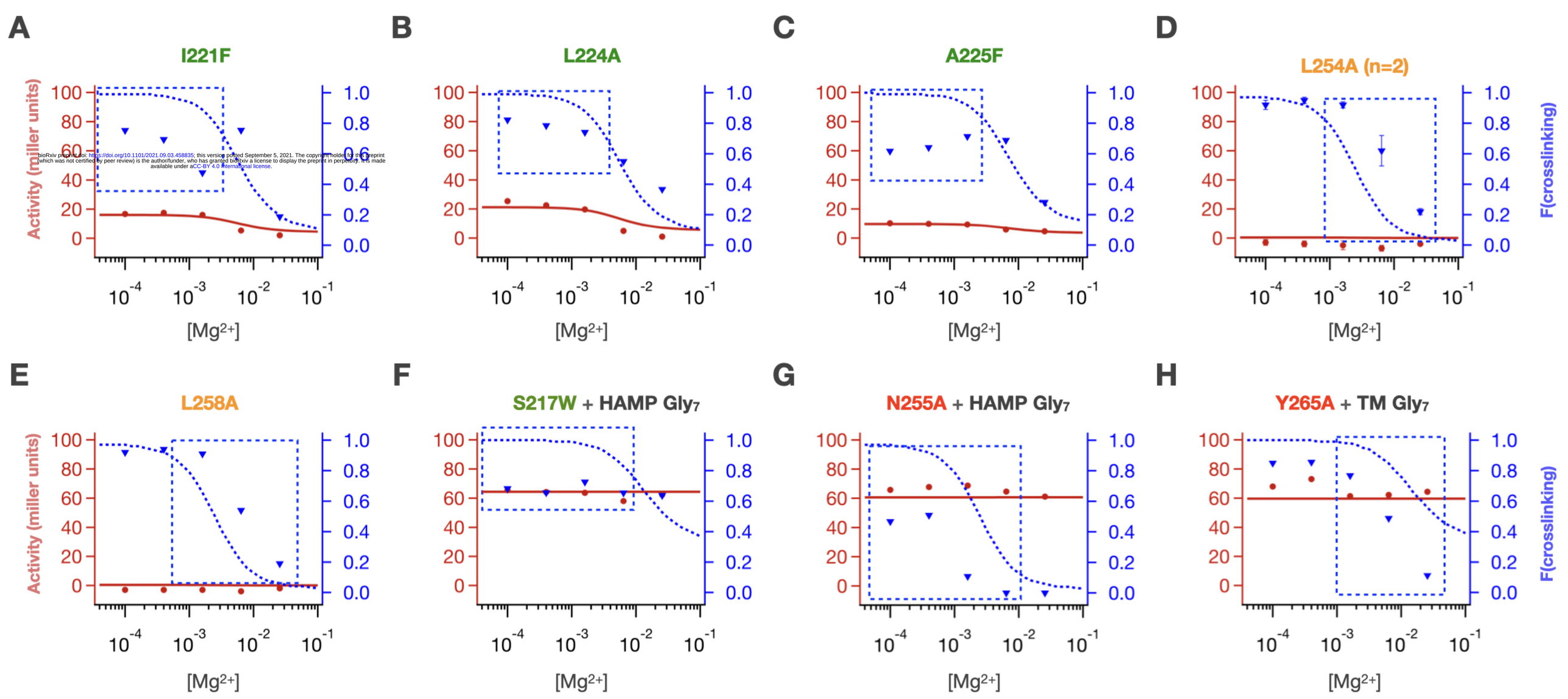

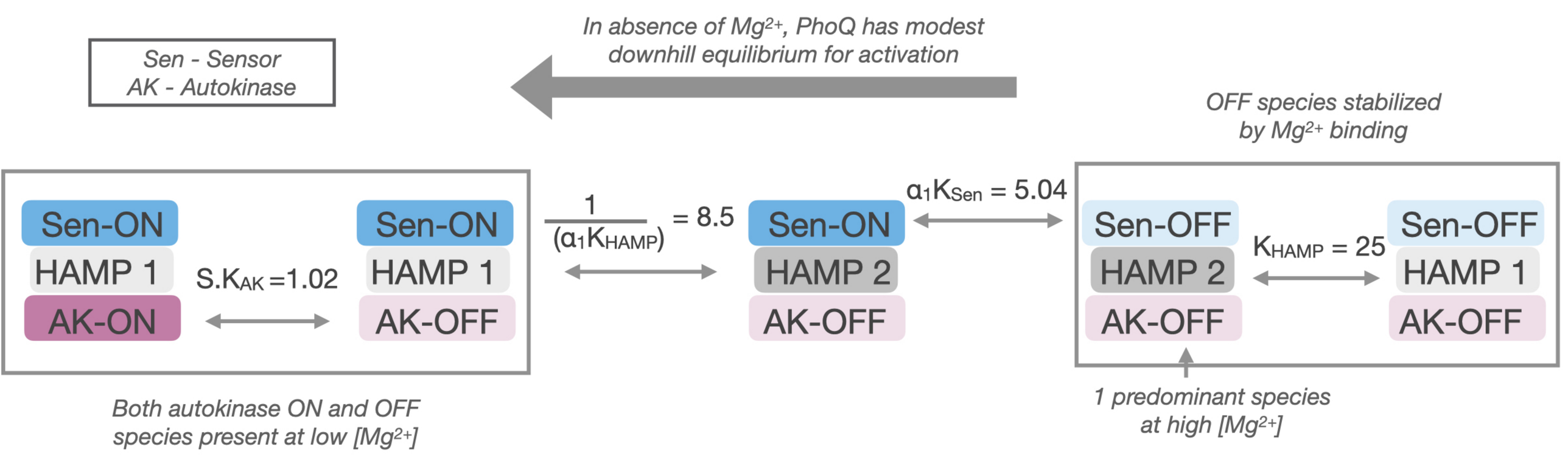
Sen - Sensor
AK - Autokinase
In absence of Mg2+, PhoQ has modest downhill equilibrium for activation
OFF species stabilized by Mg2+ binding
Sen-ON
HAMP 1
AK-ON
S.KAK =1.02
Sen-ON
HAMP 1
AK-OFF
1 / (α1KHAMP) = 8.5
Sen-ON
HAMP 2
AK-OFF
α1KSen = 5.04
Sen-OFF
HAMP 2
AK-OFF
KHAMP = 25
Sen-OFF
HAMP 1
AK-OFF
Both autokinase ON and OFF species present at low [Mg2+]
1 predominant species at high [Mg2+]